BIO-INSPIRED ALL-POLYMER 2D PHOTONIC CRYSTAL FIBERS

A THESIS

SUBMITTED TO THE DEPARTMENT OF PHYSICS

AND THE GRADUATE SCHOOL OF ENGINEERING AND SCIENCE

OF BILKENT UNIVERSITY

IN PARTIAL FULFILLMENT OF THE REQUIREMENTS

FOR THE DEGREE OF

MASTER OF SCIENCE

By

Tamer Doğan

August, 2014

I certify that I have read this thesis and that in my opinion it is fully adequate, in scope and in quality, as a thesis for the degree of Master of Science.

Prof. Dr. Mehmet Bayındır (Advisor)

I certify that I have read this thesis and that in my opinion it is fully adequate, in scope and in quality, as a thesis for the degree of Master of Science.

Assoc. Prof. Dr. Mehmet Özgür Oktel

I certify that I have read this thesis and that in my opinion it is fully adequate, in scope and in quality, as a thesis for the degree of Master of Science.

Assist. Prof. Dr. Ali Kemal Okyay

Approved for the Graduate School of Engineering and Science:

Prof. Dr. Levent Onural
Director of the Graduate School

ABSTRACT

BIO-INSPIRED ALL-POLYMER 2D PHOTONIC CRYSTAL FIBERS

Tamer Doğan
M.S. in Physics
Supervisor: Prof. Dr. Mehmet Bayındır
August, 2014

Photonic crystals are essential part of the integrated systems which require manipulation of light in a manner that all-optical polarization and reflection properties are completely calibrated to necessary levels. However, beyond scientific development of photonic crystals, biological systems also provided inspiration for the field since they perfected the mechanisms in terms of coloration over millions of years. In addition, natural samples are also observed to serve and function for more than single purpose, and this further illuminates the technological designs so as to develop multifunctional structures. *Anas Platyrhynchos L.* (mallard) is one of the natural examples and detailed investigations yield that its neck feathers have structural coloration, iridescence and hydrophobicity.

Being inspired form mallard duck, two-dimensional photonic crystal fibers are produced to imitate coloration and surface architecture. The fabrication is established by iterative size reduction technique which, as a top-down method, enables design of nano-scale materials from macro-scale structures. To accurately imitate duck feathers, polycarbonate (PC) and polyvinyldifluoride (PVDF), are characterized and selected for their thermal compatibility and dielectric properties among number of polymers.

Produced 2D photonic crystal fibers have been demonstrated to reflect color of green like duck feathers, and also shown to have iridescence by optical means. Besides single coloration, all colors of visible spectrum are also obtained to attest potential applicability of fabrication technique and produced fibers. It is also substantiated that all colors can be obtained in a single fiber by tapering a thick fiber. In addition, last but not least, 2D photonic crystal fibers are carefully designed to have surface roughness which promoted hydrophobic feature of

PVDF and provided better hydrophobicity than natural counterparts. Manufactured structures are also the first demonstration for production of all-polymer two dimensional photonic crystal fibers which may be used in textile or filtering technologies.

Keywords: Nanophotonics, Photonic Band Gap Materials, Structural Coloration, Photonic Crystal Fiber, 2D Photonic Crystal, Multifunctional Fiber, Polymer Fiber.

ÖZET

DOĞADAN ESİNLENİLMİŞ TAMAMEN POLİMER 2B FOTONİK KRİSTAL FİBERLER

Tamer Doğan
Fizik, Yüksek Lisans
Tez Yöneticisi: Prof. Dr. Mehmet Bayındır
Ağustos, 2014

Fotonik kristaller, ışığın polarizasyon ve yansıma özelliklerinin gerekli seviyelere kolayca ayarlanmasını gerektiren tümleşik optik sistemlerin önemli parçalarıdır. Ancak, fotonik kristallerin bilimsel gelişmesinden öte, biyolojik sistemler renklenme açısından bulundurdukları mükemmel mekanizmalarla bu alana ilham kaynağı olmuşlardır. Doğal örneklerin birden fazla amaca hizmet eden yapılar barındırdıkları ve bu sayede teknolojik gelişmelere çok-fonksiyonlu yapılar olarak da katkı sağladıkları gözlemlenmiştir. *Anas Platyrhynchos L.* (yaban ördeği) de bu örneklerden birisi olarak detaylı olarak incelenmesi sonucunda boyun kısmındaki tüylerin iki-boyutlu fotonik kristal renklenmesi, yanardönerlik ve hidrofobiklik özelliklerini içerdiği anlaşılmıştır.

Yaban ördeğinden ilham alınarak, bu yapıları renklenme ve yüzey özellikleri bakımından taklit eden iki-boyutlu fotonik kristal fiberler üretilmiştir. Üretim, bir yukarıdan-aşağıya metodu olan ve nano-yapıları büyük boyutlardan kontrol etmeyi sağlayan, tekrarlamalı boyut küçültme tekniğiyle gerçekleştirilmiştir. Ördek tüylerini tam olarak kopyalayabilmek için polycarbonate (PC) and polyvinyldifluoride (PVDF) malzemeleri incelenmiş, ve sıcaklık uyumlulukları ve dielektrik özelliklerinden dolayı birkaç polimer arasından seçilmişlerdir.

Üretilen 2B fotonik kristal fiberlerin ördek tüyleri gibi yeşil renkte yansıdıkları ve yanardönerlik özelliğine sahip oldukları optiksel olarak gösterilmiştir. Tek rengin yanında, görünür tayfın bütün renklerini yansıtan fiberler de elde edilerek fabrikasyon tekniğinin ve üretilen fiberlerin potansiyel uygulanabilirlikleri beyan edilmiştir. Ayrıca bütün renkler kalın bir fiber inceltilerek tek bir fiber üzerinde gösterilmiştir. Son fakat aynı derecede önemli olarak da 2B fiberler dikkatlice üzerlerinde yüzey pürüzlülükleri olacak şekilde dizayn edilmiştir ve bu sayede PVDF malzemesinin hidrofobik özelliği doğal yapıyı geçecek kadar geliştirilmiştir.

Elde edilen yapılar bu zamana kadar üretilen tamamı polimer 2B fotonik kristal fiberlerin ilkidir ve tekstil ve ışığı süzme teknolojilerinde kullanılabilirler.

Anahtar sözcükler: Nanofotonik, Fotonik Band Aralıklı Malzemeler, Yapısal Renklenme, Fotonik Kristal Fiber, 2B Fotonik Kristal, Çok Fonksiyonlu Fiber, Polimer Fiber.

Acknowledgement

I am very thankful to my superviser, Prof. Dr. Mehmet Bayındır, for his patience, encouragement and inspiration on this thesis. He introduced me to scientific world and helped me to develop an understanding of the working mechanisms behind scientific processes.

I would like to especially thank to Dr. Tural Xudiyev for his instructive talks. I have worked with him throughout my thesis process and he has been like a second advisor for me. I have learned variety of experimental methods from him and I have been envisioned by his experiences.

I acknowledge that it was an honour to meet Dr. Gökçen Birlik Demirel during my master's thesis years. I feel quite lucky to have a chance to work with her and know her. She has been an instructor, an advisor, a colleague and a friend to me. Her contribution on my personal development, on my scientific career and on my life shall and will never be forgotten.

I additionally would like to acknowledge my thanks to Pınar Beyazkılıç, Muhammad Yunusa, Urandelger Tuvshindorj and Emre F. Öztürk for their presence as friends and colleagues in the time of need. I am exclusively thankful to Mrs. Nese Özgür and Mr. Murat Dere for being unique coordinators in this group. I would like to additionally acknowledge my thanks to other (former) group members Ozan Aktaş, Tuğrul Cinkara, Dr. Osama Tobail, Ersin Hüseyinoğlu, Pelin Tören, Erol Özgür, Adem Yıldırım and Bihter Dağlar. Besides group members, I would like to thank my supportive friends Özer Duman, Yazgan Tuna, Samet Akpınar and Burak Gököz.

In addition to group members I would like to thank both Prof. Salim Çıracı and Prof. Mehmet Bayındır for their effort on foundation of National Nanotechnology Research Center (UNAM).

Finally, I am very grateful for endless moral support of my family. I would not be able to complete this work without their unique presence and support. I

dedicate this thesis to my brothers both in blood and bone: Kadir Doğan and İskender Doğan.

Contents

1 Introduction **1**

2 Theoretical Backgorund **4**

2.1 Photonic Crystals 4

2.1.1 Review of Photonic Crystals 5

2.1.2 Photonic Crystals in Nature 13

2.2 Functional Surfaces 21

2.2.1 Review of Smart Surfaces 21

2.2.2 Multi-Functional Surfaces on Plants and Animals 24

3 Fiber Design and Fabrication **28**

3.1 Iterative Size Reduction Method 29

3.2 Material Characterization and Preform Preparation 34

3.3 Design and Fabrication of Novel Preforms and Fibers 39

3.3.1 2D Photonic Crystal Fibers 40

4 Fiber Characterization **43**

4.1 2D Photonic Crystal Fibers For Bio-Mimicry of Anas Platyrhynchos L. 44

4.1.1 Optical Characterization of Bio-inspired Fibers 44

4.1.2 Surface Behaviour Characterization 50

5 Conclusion and Future Work **54**

List of Figures

2.1 Examples to 1D, 2D and 3D photonic crystals. Each structure is periodic in different number of directions. Photonic crystals are usually made out of two different materials which are represented by diversity in colors. Adopted from Ref. 25. 5

2.2 Isotropic and homogeneous layer of dielectric medium. 6

2.3 Cross-section of photonic bandgap (PBG) fiber. As it can be seen, several layers of one-dimensional photonic crystal is located at the inner surface of the fiber. Adopted from; Ref. 39. 7

2.4 An example of a band diagram for two-dimensional photonic crystal. Here, dielectric rods that have dielectric constant of 8.9 are assembled in a square lattice formation with $r/a = 0.2$. Adopted from Ref. 25. 9

2.5 SEM and optical images of various 2D photonic crystal fibers. Adopted from Ref. 47. 11

2.6 Preparation procedure for Yablonovite type three-dimensional photonic crystal. Adopted from Ref. 49. 12

2.7 Structural coloration examples from nature. 13

2.8 Quasi-multilayer structures on the wing scales of *Morpho didius* butterfly. Tree-like formation is biologically favoured since it is required for them to grow from only one location. Adopted from Ref. 53. 15

2.9 Peacock feathers are formed by square lattice arrangements of melanin rods in a keratin matrix. Adopted from Ref. 12. 16

2.10 Bright-green coloration and iridescence on neck feathers of Mallard duck. Hexagonally distributed melanin rods at the edge of the barbules cause coloration through 2D photonic crystal effect. . . . 17

2.11 Band diagram and reflection simulations further supports 2D photonic crystal effect as the cause of coloration. Very good match between reflection measurement and simulation proves melanin rod size and hexagonal distribution. 19

2.12 SEM images and reflection measurement from beetle samples. a) Assembly of particles and linkup between them suggest 3D photonic crystal effect. b) Reflection measurement from *Glenea celia*. c) SEM images for *Eudiagogus pulcher* shows 3D structure formed out or layers. Adopted from Ref. 55. 20

2.13 Contact angles according to different surface energy correlations. . 22

2.14 Microstructures on Lotus leaf are found to consist nano-pillars which promote hydrophobicity even further. Adopted from Ref. 72. 25

2.15 Feathers are found to possess (besides coloration), self-cleaning property which is considered to be emphasized by hierarchical roughness. 27

3.1 Schematic for iterative drawing procedure is shown. Resulting fiber cross-section and longitudinal SEM images are given. This technique helps to fabricate very long nanowires in desired orientation. Adopted from Ref. 85. 31

3.2 Home-built fiber tower used for iterative size reduction. 33

3.3 Band diagram and reflection simulations carried out before drawing procedure to estimate required rod sizes. 35

3.4 Home-built consolidator and prepared first step preform. 37

3.5 Schematic for first step drawn preform and real preform are given. As it is clearly observed from SEM images, fibers preserved their cross-sectional ratio throughout the drawing process. 38

3.6 Real and schematic second step preform are given. Cross-section of second step possess hexagonally distributed micro-scale rods. . 40

3.7 Only single fiber is inserted into third step preform since it is just aimed to decrease its overall size. 41

4.1 Photograph of optical setup. Mechanism used can be understood from schematics. 45

4.2 Green fibers show iridescent behaviour under higher magnification and the idea of matching between measurement and simulation further approves coloration due to photonic crystal effect. 46

4.3 Adjusting to different lattice constants any wavelength can be reflected by 2D photonic crystal. 47

4.4 Using map ř efcolormap for producing different wavelengths, colors of visible spectrum are produced. 48

4.5 Single fiber can be tapered in a segment as small as 1 mm to reflect all visible spectrum. 49

4.6 Contact angle setup gives an edge to analyse hydrophobic feature of the samples. 50

4.7 Contact angle measurement from assemble of final photonic crystal fibers. 51

4.8 Contact angle measurements taken both from film PVDF and second step photonic crystal structure. 52

List of Tables

3.1 Polymer materials 34

Chapter 1

Introduction

Most of the colors we observe in nature are produced either due to pigments which function by absorption of variety of wavelengths or via structural coloration that results from interaction of light with structures that have sizes comparable to operated wavelengths [1, 2, 3]. Pigments are structures with certain chemical compositions which can be produced artificially and highly observed on natural surroundings [4]. On the other hand, structurally colored structures are outcomes of meticulously integrated materials with specifically arranged physical properties [5]. In the light of this point of view, structural coloration have drawn great attention both for its capability for wide variety of applications such as integrated optics, display technologies etc. and for its amazing examples found in nature for which scales of butterfly wings and feathers of certain types of birds can be given as two instances [6].

Structural coloration is usually observed and investigated in the living systems, and it is considered to function for several purposes such as camouflage, mate attraction, UV protection and so on [7, 8, 9]. Among the range of structural coloration strategies found in nature are: diffraction gratings, photonic crystals, scattering etc. The most studied and imitated coloration methods are photonic crystals which are especially notable for their iridescence and exceptionally bright coloration [10, 11, 12, 13]. In the first part of the consequent chapter of this theses, theoretical background that is necessary for calculation of optical properties

of photonic crystals is given. Furthermore, influence of small perturbations and effects of changes in symmetry are covered.

Although photonic crystals are experimented and physical phenomena behind them are understood long before they were observed from natural samples [14], most of the attention was drawn after detailed investigation of natural photonic designs through scanning and transmission electron microscopes (SEM and TEM). Particular and distinct coloration designs observed on variety of natural structures are largely explored by many research groups [15, 16]. As correspondence to this end, photonic crystal examples from nature are further focused in the next chapter. In addition to instances from literature, our work on detailed investigation of bright and iridescent green neck feathers of *Anas Platyrhynchos* (mallard drakes) is also clarified in that chapter.

Beyond color production most of the natural samples are found to possess different characteristics which apparently serve to function more than simple color trend. Those multi scaled architectures are commonly known as 'multifunctional' structures and they exhibit distinct properties such as self-cleaning, superhydrophobicity, adhesion, anisotropic wettability and more of which may remain unexplored [17, 18]. Our investigation displays superhydrophobicity in addition to bright coloration, therefore on account of this, smart surfaces and multifunctional surfaces on plants and animals including our hydrophobic characterization of feather samples are examined in another section of Chapter 2.

Further development in this area was accomplished by successful imitation of investigated structures with certain materials and precise parameters. To produce structures that work consistently, lots of fabrication methods have been proposed and some survive to this date as they satisfactorily mimic the exact structures. In particular for photonic crystals, a few fabrication methods such as self-assembly or deposition techniques manage to mimic nature-inspired 1D and 3D photonic crystals [19, 20], but functional imitations of 2D photonic crystals observed in nature are yet to be produced. In respect with this point, this thesis mostly concerns about exact imitation of green head feathers of investigated *Anas Platyrhynchos*. Used fabrication technique, compatible material selection,

and design, modification and construction of two-dimensional photonic crystal fibers including theoretical calculations necessary for optimization of each process are thoroughly explained in Chapter 3.

In recent years, fabrication techniques have preceded beyond copying the original structures, and present phenomena have been further modified as required for integrated systems, important instances of which can be given as Bragg fibers, anti-reflective coatings, waveguides etc [21, 22, 23, 24]. Production for most of the mentioned structures necessitates adjustment of the fabrication procedures since versatility is considerably essential for these systems to accommodate with current technology. This study was shaped taking this progression into account and thus resulted in more than single colored fibers. In the last section of Chapter 3, processes and procedures considered for fabrication of colorful fibers are explained. Further optical and surface characterization of two dimensional photonic crystal fibers are described in Chapter 4. Novelties and facilities offered by bio-inspired all-polymer photonic crystal fibers are discussed in the last chapter.

Chapter 2

Theoretical Backgorund

2.1 Photonic Crystals

Photonic crystals are periodic structures that are used to manipulate the propagation of light with certain wavelength(s) [25]. There are three specific photonic crystals: one-, two- and three-dimensional photonic crystals (Fig 2.1). Number of directions that possess periodicity determines type of photonic crystal (e.g. 1D photonic crystals are periodic in one direction where 2D PC are in two directions and etc.) Photonic crystals contain at least two distinct materials that differ in optical properties, especially in refractive indices. When those specific materials are periodically arranged, they form particular band gap arrangement for which explicit frequencies of light that satisfies resulting conditions can travel through or get reflected from the structure.

Photonic crystals are not only checkpoints for particular frequency range but also can be arranged to check polarization of incident light [26, 27]. This property can be more prominent in 2D photonic crystal since some polarizations of incoming light will eventually face nonsymmetric configuration and will not experience the effect of periodicity [28, 29]. On the other hand, some structures can be utilized in favor of technology in a way that they prevent all polarization of specific range of wavelengths via complete photonic band gaps.

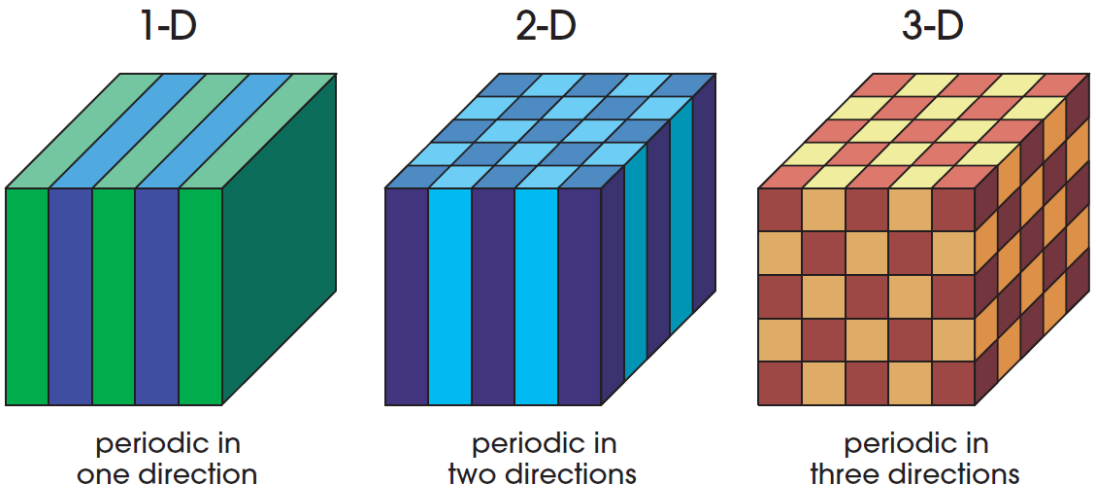

Figure 2.1: Examples to 1D, 2D and 3D photonic crystals. Each structure is periodic in different number of directions. Photonic crystals are usually made out of two different materials which are represented by diversity in colors. Adopted from Ref. 25.

2.1.1 Review of Photonic Crystals

2.1.1.1 One-dimensional photonic crystals - Multilayer films

The concept of photonic crystals bases back to 1887 when Lord Rayleigh published his first studies on multi-layer stack of dielectric materials [14]. He explained the working mechanism by accurate calculations on that first 1D photonic crystal. The main idea that corresponds to complete reflection of incident light from multilayer dielectric mirror is that periodic arrangement and thickness of the layers are comparable to the operated wavelength in a way that multiple reflection of forward travelling wave interferes destructively [30]. The simple correlation between spacing and wavelength for omnidirectional reflection is given as

$$d = \frac{\lambda}{4n_i} \tag{2.1}$$

where λ is wavelength in free space and n_i is the refractive index of alternating materials. Such one-dimensionally periodic structures are also known as quarter

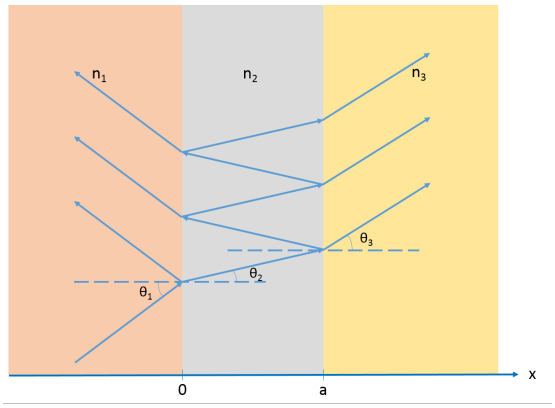

Figure 2.2: Isotropic and homogeneous layer of dielectric medium.

wave stack and reflection can be calculated using following equation

$$R = \tanh^2\left(N \ln \frac{n_1}{n_2} + \frac{1}{2} \ln \frac{n_s}{n_0}\right) \tag{2.2}$$

where n_0, n_s are refractive indices of starting and ending mediums, n_1, n_2 are refractive indices of respective dielectric layers, and N is the number of pair layers. This equation clearly states that reflectivity reaches unity as number of layers increases, however usually 6-8 pairs are good enough to approach 99% reflectivity for most of the materials. This sort of multilayer configurations are widely used in many of the current devices.

On the other hand, some technological requirements necessitate controlled reflection and transmission percentages of electromagnetic waves rather than fully reflecting mirrors [31, 32, 33]. For this purpose, proper reflection coefficient for basic 1D photonic crystal can be calculated with not so complicated electromagnetic treatment. Considering simple, isotropic and homogeneous layer as in Fig 2.2 with refractive index function

$$n(x) = \begin{cases} n_1, & \text{if} \quad x < 0 \\ n_2, & \text{if} \quad 0 < x < a \\ n_3, & \text{if} \quad a < x \end{cases} \tag{2.3}$$

One can calculate the reflectivity of this medium with transfer matrix method and find

$$R = \left|\frac{A}{B}\right|^2 \tag{2.4}$$

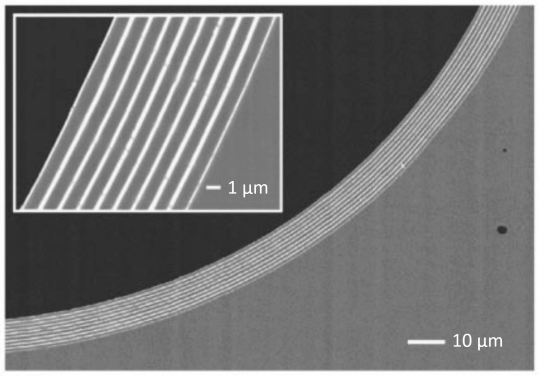

Figure 2.3: Cross-section of photonic bandgap (PBG) fiber. As it can be seen, several layers of one-dimensional photonic crystal is located at the inner surface of the fiber. Adopted from; Ref. 39.

where A and B are given by

$$A = \frac{1}{2}\left(\frac{\cos\,\theta_3}{\cos\,\theta_1} - \frac{n_3}{n_1}\right)\cos\,\phi \;-\; \frac{i}{2}\left(\frac{n_2\,\cos\,\theta_3}{n_1\,\cos\,\theta_2} - \frac{n_3\,\cos\,\theta_2}{n_2\,\cos\,\theta_1}\right)\sin\,\phi\;,$$
$$B = \frac{1}{2}\left(\frac{\cos\,\theta_3}{\cos\,\theta_1} + \frac{n_3}{n_1}\right)\cos\,\phi \;+\; \frac{i}{2}\left(\frac{n_2\,\cos\,\theta_3}{n_1\,\cos\,\theta_2} + \frac{n_3\,\cos\,\theta_2}{n_2\,\cos\,\theta_1}\right)\sin\,\phi\;. \tag{2.5}$$

Here, ϕ is the phase shift of the light which is described by

$$\phi = \frac{2\pi n_2 a}{\lambda}\,\cos\,\theta_2 \tag{2.6}$$

By changing mediums and stacking them periodically with different thicknesses desired reflectivity values can be set. There are huge number of examples in the literature for such layered media schemes to be used in variety of purposes and applications. For instance, in the fiber technology, 1D photonic crystals can be axially integrated along the fibers to guide the selected wavelengths of incident spectrum [34, 35]. Particular example for this kind of fibers can be given as photonic band gap fibers [36, 37, 38]. These fibers transmit the incoming light regardless of its incident angle as long as it is headed inside the hollow core of the fiber. Additionally, bending the fiber does not result with loss of efficiency since reflection from inner surface is omnidirectional. A cross section SEM image for this type of fiber can be seen in Fig 2.3.

Temelkuran *et. al.* reports that this fibers can guide high power CO_2 laser with wavelength of 10.6 μm [39]. High power feature is due to hollow core structure because solid core fibers start to heat after a while or non-linear effects take place and those problems cause fiber not to function properly. Coaxially layered media in the figure includes materials of arsenic selenide (As_2Se_3) and polyethersulfone (PES) that are stacked periodically with respective thicknesses of As_2Se_3 and PES.

This sort of fibers are currently in use for various medical applications from orthopaedic surgery to photodynamic therapy since they can deliver high power lasers smoothly without any loss while bending [40, 41]. However, beyond fiber technology, 1D photonic crystals found themselves very wide range of range applications such as Bragg reflector lasers, colorful fibers, laser delivery systems etc [42, 19, 34].

2.1.1.2 Two-dimensional photonic crystals

First approach to and demonstration of 2D photonic crystals was made by Krauss *et. al.* in 1996 [43]. In that paper, holes were drilled in hexagonal arrangement on a semiconductor substrate and final structure resulted in polarization dependent photonic band gap. It was also shown that as the angle of incidence varied the transmission spectra changed drastically. The corresponding angle for this change was polarization dependent.

The most important property of all 2D photonic crystals regardless of which lattice arrangement is employed is its iridescence [44, 45]. Iridescence is the occurrence of a shift on the reflected wavelength as the angle of illumination changes. This is usually caused due to adjustment of the band gap; it might either move towards different frequencies or shrink/enlarge in width. Therefore, in 2D photonic crystals incident angle, frequency and polarization of the light decides the reflected wavelength since those features respectively modify lattice constants, material indices and periodic arrangements.

As an instance to iridescence, band diagram for square lattice 2D photonic

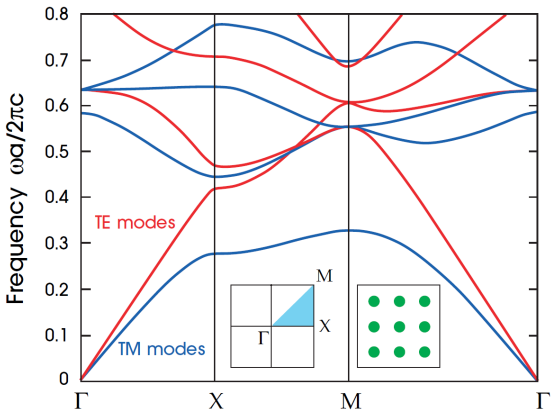

Figure 2.4: An example of a band diagram for two-dimensional photonic crystal. Here, dielectric rods that have dielectric constant of 8.9 are assembled in a square lattice formation with $r/a = 0.2$. Adopted from Ref. 25.

crystal is given in Fig 2.4. This specific lattice have radius to lattice constant (r/a) ratio of 0.2. Materials are cylindrical rods with dielectric constant of 8.9. It is apparent that there is band gap for only TM polarization (blue lines). In addition, graph also informs about how band gap shrinks and shifts as the angle of view changes from M to K which are points in the brillouin zone shown in the inset. However this is not always the case, changing materials and radius to lattice ratio, it is possible to form different band gap configurations.

Since photonic band diagrams are invariant under frequency and lattice constant change, corresponding wavelength for specific frequency locations can be obtained by the very simple equation given as

$$\frac{c}{a} = \frac{c}{f\lambda} \tag{2.7}$$

Thus in this case, relation between frequency and lattice constant is

$$\frac{a}{\lambda} = f \tag{2.8}$$

For the given diagram, the gap center is around 0.4, then the corresponding wavelength for lattice constant $a = 200$ nm is $\lambda = 500$ nm. This sort of 2D photonic crystals can be used for waveguiding purposes or localization of specific modes.

On the other hand, 2D photonic crystals is also commonly used in fiber technology as waveguides. First 2D photonic crystal fibers were produced by P. Russell and his group to guide the light using total internal reflection (TIR) [46]. TIR is a reflection mechanism when light hits the surface with an angle larger than critical angle and gets completely reflected. The critical angle is simply given by Snell's law for which refraction angle is 90^o

$$\frac{\sin\,\theta_c}{\sin\,90} = \frac{n_1}{n_2} \qquad \Rightarrow \qquad \sin\,\theta_{critical} \geq \frac{n_1}{n_2} \tag{2.9}$$

where n_1 and n_2 are refractive indices of materials through which light passes respectively.

The fiber was formed of regular and doped silica, and produced by drawing technique [47]. Preform is prepared by bundling silica tubes in hexagonal arrangement then fusing them into glass formation. Preform can have a solid (non-tube) core and hollow (regular) core depending on requirements (Fig 2.5). First reported 2D photonic crystal fiber was a solid core and it was guiding both single mode and multi mode waves based on diameter of the holes (d). It was shown that fundamental mode is guided for configurations where $d/\lambda < 0.4$. Therefore, by doping solid core (e.g. with Germanium) and by taking advantage of guiding condition, fibers that guide multi modes can be prepared. This type of fibers can yield high power laser waveguides since light confines pretty well inside the fiber.

This thesis is focused on two-dimensional photonic crystal fibers. However, there are many basic differences between fibers formed here and explained above. Firstly, bio-inspired fibers are proposed for coloration effects rather than waveguides, in other words, observation in radial axis is prominent rather than cross-section details. In addition, materials used here are high temperature polymers which are selected to enrich imitation. Also, last but not least, solid core, for above formation, means the single fiber right in the middle of the cross-section, however, in our configuration solid core means that each of the hollow tubes are filled with different material which completely covers that hollow. Properties of our fiber will be explained in more detail in following chapters.

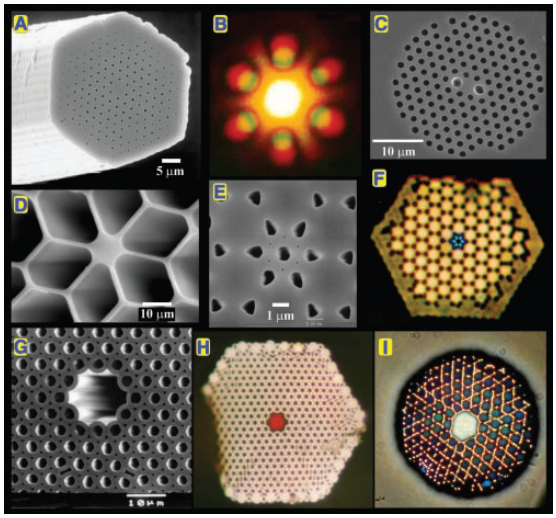

Figure 2.5: SEM and optical images of various 2D photonic crystal fibers. Adopted from Ref. 47.

2.1.1.3 Three-dimensional photonic crystal

The term 'Photonic Crystal' was first used by Yablonovitch in 1987 [48]. He coined this term to such structures that are used for measurement and control of electromagnetic waves and shortly described them as semiconductors of light since they can transmit or reflect light with certain and precise conditions. Yablonovitch's real contribution to the field was production of the first three-dimensional photonic crystal with a complete photonic band gap [49]. He and his team produced centimeter scale diamond like (not exactly diamond configuration) structure that has band gap width around 0.09 and centered at 0.535 frequencies. The structure itself is shown in Fig 2.6.

Although the first laboratory investigation and fabrication of 3D photonic crystal structure was accomplished by Yablonovitch and his team, the first calculations were made a year before that [50]. As reported by Ho et. al., arrangement of high dielectric spheres in a diamond lattice configuration forms complete photonic band gap. That paper was purely based on calculation of band diagram for such structures using plane-wave expansion method. In addition, diamond lattice here actually corresponds to regular diamond formation but with large spheres that eliminate necessity for any bonds to connect them.

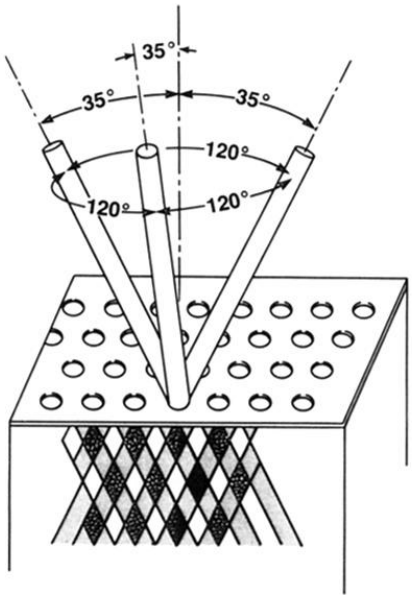

Figure 2.6: Preparation procedure for Yablonovite type three-dimensional photonic crystal. Adopted from Ref. 49.

There are further more creative and unique 3D photonic crystal examples that show remarkable properties and some of them include defects inside to localize electromagnetic waves or some modes. All photonic crystals are distributed among many research areas and technological devices and they still help to improve the overall progress in important fields such as optoelectronics, textile and display technologies.

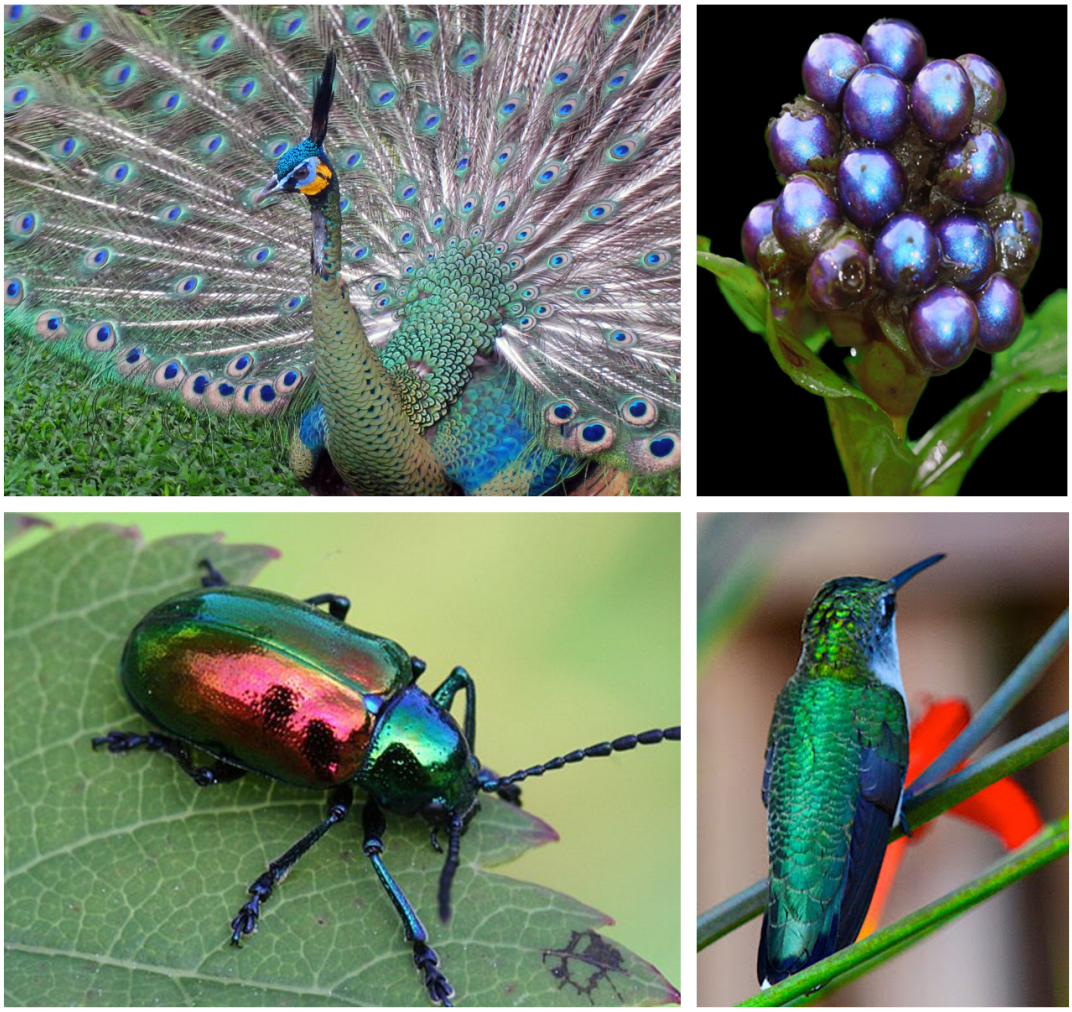

Figure 2.7: Structural coloration examples from nature.

2.1.2 Photonic Crystals in Nature

As coloration mechanisms from natural samples were started to be investigated through the invention of electron microscopes (SEM,TEM etc.), it was found that photonic crystals were as common as pigments. In short, pigments are chemical compounds that selectively reflect or transmit certain range of wavelengths of incident light. It is not only that photonic crystals are periodically structured materials but also different and clever designs in biological systems made the analysis of this field more attractive. In addition, exact wavelength or polarization to be reflected can be adjusted with small error margin in photonic crystals,

however pigments can only give colors at a level that they are distinguishable by human eye. Mostly, observed photonic crystals promise new formations and different iridescence properties to be used in technology.

One of the most celebrated photonic crystal configuration in a natural sample is found in the wing of butterflies [16, 51, 52]. A considerable example can be bright, blue coloration in *Morpho didius* [53]. A detailed optical investigation of wing scales of this particular insect was first investigated in 1999. Vukusic *et. al.* reported the exact microstructures responsible for coloring and the mechanism that enables visibility in wide range of angles. As the structural coloration, in *Morpho* butterfly there is one-dimensional photonic crystal that includes keratin and air. Since air is not solid it is not easy task to use it in 1D photonic crystal without a compromise. Therefore as a design, this structure became a remarkable example. As can be seen in Fig 2.8, the wing scale includes multi-layer structure formed of air and keratin by separating solid layers with a fundamental column. It is also worthy to note that there is not any complete formation. In other words the structure is not exactly 1D photonic crystal, it includes multi-layers in the form of trees. In addition, keratin layers get thinner as it grows away from the column. And last but not least, distance among tree structures, periodicity on larger scales also contributes to the total reflection and iridescence. Although the micro structures fade away from ideal photonic crystal, their bright coloration and iridescence feature shows that the two distinguishing properties make the wing scales a distinct architecture rather than an inaccurate design.

Optical characterization of the wing structure mostly concerns about transmission and reflection from single scales. Present photonic crystal is not periodic in the other plane, therefore it does not exhibit similar reflection amount corresponding to angle change. They reported high reflection to be effective for angle range larger than 100° through periodic plane, on the other hand range of only 15° is operating for vertical plane. To see full effect from reflection and transmission, they characterized and took measurements with 488 nm TM polarized light. Their claim for high reflection, up to 75%, at even large angles is that a transparent layer above the photonic crystals causes diffraction of light. In addition, it is discussed that reflection could reach 100% if the spacing among trees

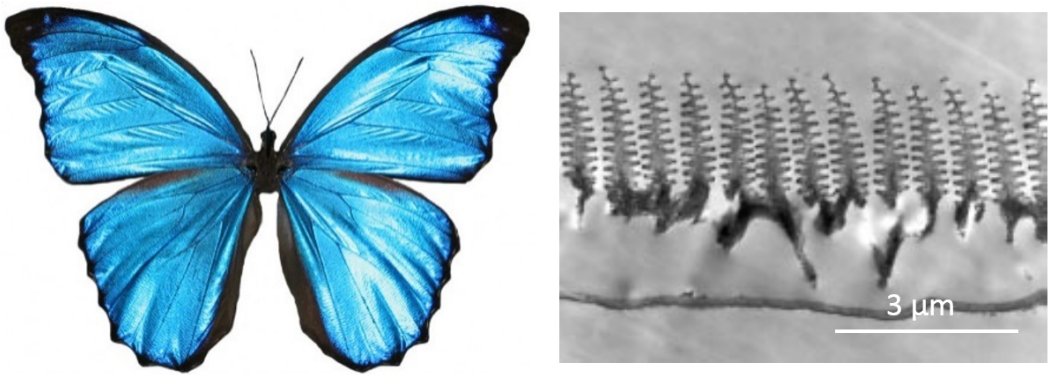

Figure 2.8: Quasi-multilayer structures on the wing scales of *Morpho didius* butterfly. Tree-like formation is biologically favoured since it is required for them to grow from only one location. Adopted from Ref. 53.

matches quarter of the wavelength which is not the case in the wing.

Realization of two-dimensional photonic crystal in a natural sample was first reported in 2003, explaining coloration strategies in peacock feathers [12]. It was shown by electron microscope images (Fig 2.9) that there exist a square lattice of rods distributed in the feathers of *Pavo muticus* peacock. With necessary simulations, they demonstrated that partial photonic band gap is responsible for reflection of light with specific wavelength from barbules. Since investigated peacock feathers include variety of colors, how lattice properties changes among differently colored barbules is also explained.

According to their findings, there are two main mechanisms that help to alter the color. First one is the lattice constant which usually affects the location of the band gap directly, so that it results with reflection of different frequencies. The more uncommon feature of this structural coloration is number of periods. It is stated that as number of periods decrease reflected range of frequencies increases, thus different colors start to mix. Found lattice constant for colors of blue, green and yellow were 140, 150 and 165 nm and number of periods stated to be 9, 6 and 4, respectively.

Our inspiration to produce all-polymer solid core two-dimensional photonic crystal comes from particular structural coloration example of mallard duck [54].

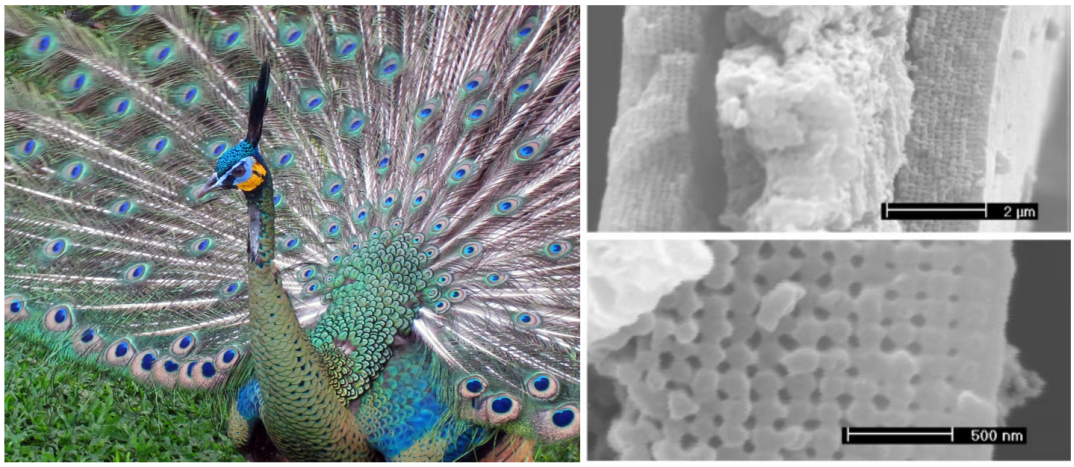

Figure 2.9: Peacock feathers are formed by square lattice arrangements of melanin rods in a keratin matrix. Adopted from Ref. 12.

We have carried out detailed investigation of *Anas Platyrhynchos* which is mostly celebrated for its brightly colored green head feathers. Apart from single coloration, it also possesses iridescence property that either correspond to color shift to blue or total disappearance of the present color. Optical characterization of the feathers clearly manifests this iridescence. As it can be seen in Fig 2.10, originally green looking barbule switches its reflected color to blue as the angle range from which light increases. Optically, this was accomplished by increasing magnification of the objective because higher valued lenses gets closer to the sample and that causes rise in the percentage of accumulated light from higher angles. After this, we took variety of scanning electron microscope images to reveal both longitudinal and cross-sectional configuration both of which might contribute to the overall coloration. Apparently, mallard neck feathers are formed of well-aligned hexagonal two-dimensional photonic crystals that are deployed along edges of the barbule. A considerable fact is also observed from the barbules that they have rectangular cross section and this reasonably explains iridescence and overall coloration since specific color can be seen only in one direction and that direction is sort of multiplied along the long edge. In other words, the barbule offers continuous 2D photonic crystal by maximizing the functional surface areas of the barbule elements responsible for iridescent coloration. The main rod materials are found to be melanin which has refractive index value around 2 and they are embedded

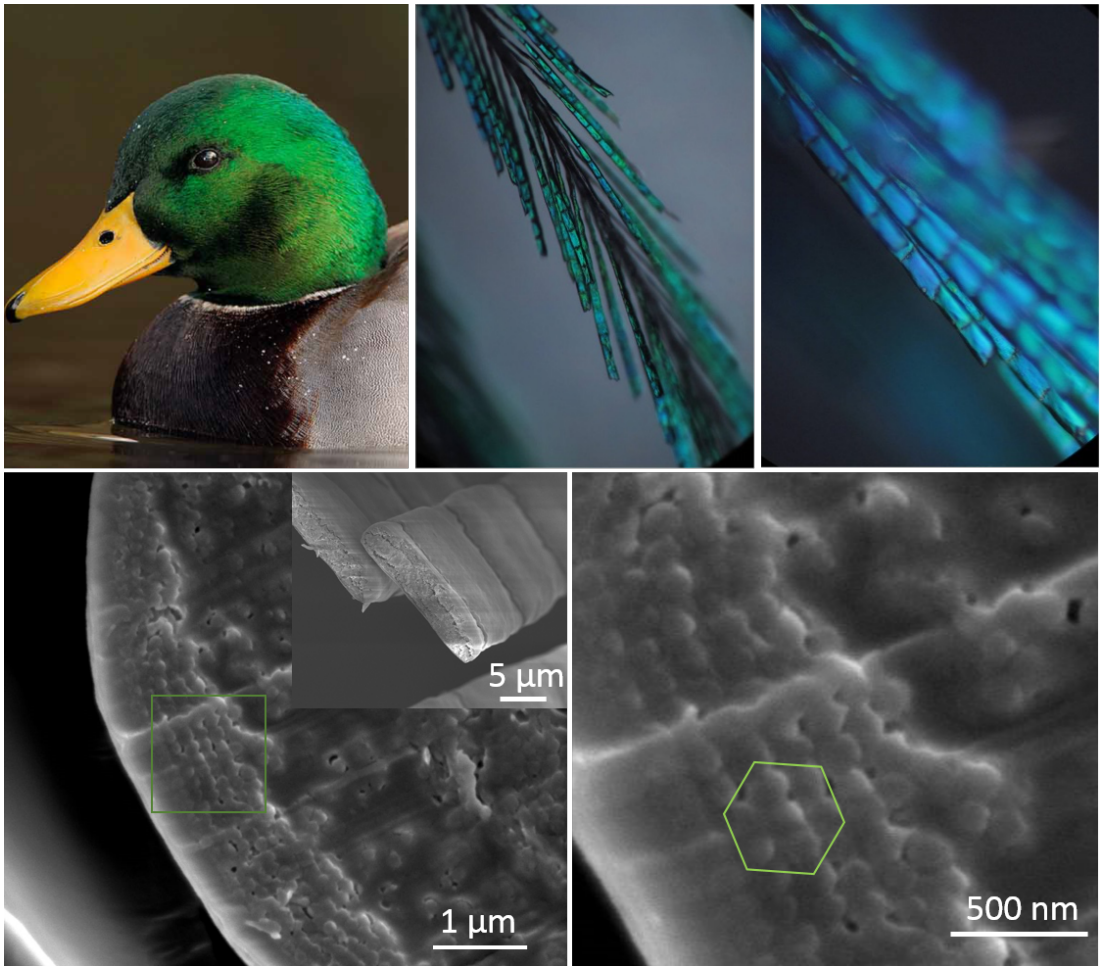

Figure 2.10: Bright-green coloration and iridescence on neck feathers of Mallard duck. Hexagonally distributed melanin rods at the edge of the barbules cause coloration through 2D photonic crystal effect.

in keratin matrix refractive index of which is 1.56. Another important parameter which is expected to contribute highly on the coloration is radius to lattice ratio. This ratio is simply divides radius of each rod to the lattice constant of the crystal formation and it helps to configure the photonic band diagram of the crystal. In our case, duck head feathers found to have radius to lattice ratio of $r/a = 65/150 = 0.433$ which is deduced from SEM images seen in Fig 2.10. Using this ratio and refractive indices we produced a band diagram of this 2D photonic crystal using MPB (Mit Photonic Bands) software which is available for free. In Fig 2.11 this diagram is plotted and as expected iridescence is substantially prominent.

It is clearly seen that as direction of the view altered the apparent color changes. We can find the corresponding wavelengths for those directions from the diagram by using equation

$$\frac{wa}{2\pi c} = f \qquad \Rightarrow \qquad \frac{a}{\lambda} = f \qquad \Rightarrow \qquad \lambda = \frac{a}{f} \tag{2.10}$$

where f is the position of the midgap in the diagram and a is the lattice constant. From the diagram, we find that position of the band gap is 0.3 in one end and 0.35 in the other, so the unitless frequency changes among those values as the direction of view altered. Putting those values and lattice constant of 150 nm to the above equation give us wavelengths as following:

$$\lambda_1 = \frac{150}{0.3} = 500\ nm \qquad \lambda_2 = \frac{150}{0.35} = 430\ nm$$

Those values correspond to colors of green and blue both of which were observed in the optical microscope as magnification altered. Thus this diagram further supports the idea that coloration exists due to photonic crystal effect. Also, reflection simulation from continuous 2D photonic crystal with given parameters produces high reflection at green wavelengths matching found values from the band diagram (Fig 2.11b). Last but not least, we took reflection measurements from green barbules using spectrometer that takes light and plots of that light's spectrum and we see that the consistency of our simulation and measurement results further supports the notion that the presence of 2D photonic crystals is responsible for the green color displayed by feather barbules (Fig 2.11c).

Colorations on exoskeleton of beetle scales can be given as examples for three-dimensional photonic crystals which are usually formed by disordered assembly of

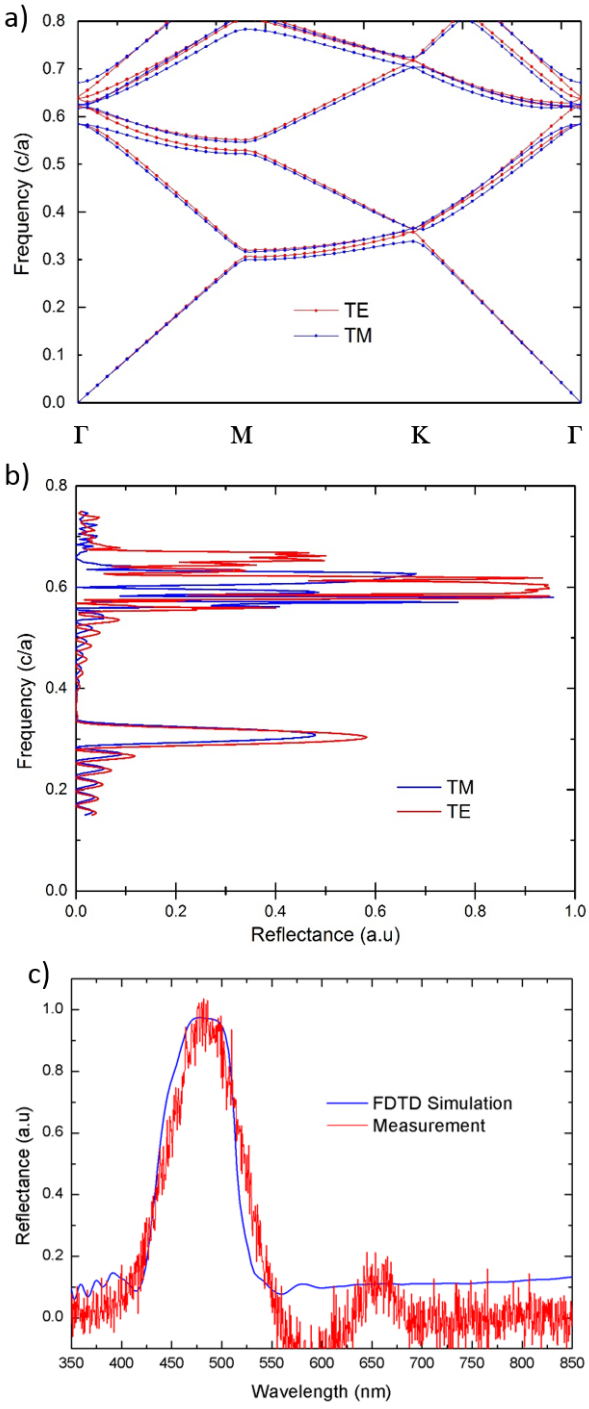

Figure 2.11: Band diagram and reflection simulations further supports 2D photonic crystal effect as the cause of coloration. Very good match between reflection measurement and simulation proves melanin rod size and hexagonal distribution.

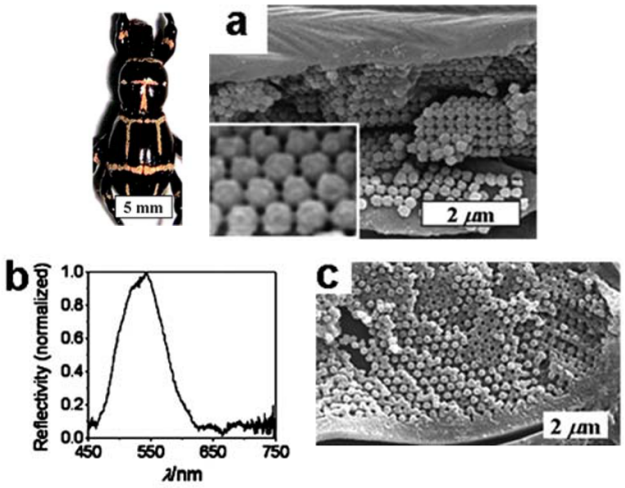

Figure 2.12: SEM images and reflection measurement from beetle samples. a) Assembly of particles and linkup between them suggest 3D photonic crystal effect. b) Reflection measurement from *Glenea celia*. c) SEM images for *Eudiagogus pulcher* shows 3D structure formed out or layers. Adopted from Ref. 55.

nano-sized spheres or non-close packed diamond lattices [11, 55]. Galusha *et. al.* reported optical and structural characterization of such structures on biological samples and they state that for *Glenea celia* spheres with diameter of 230 nm are assembled in non-close packed face centered cubic orientation to produce color of green that has reflectivity response centered around 540 nm wavelength with full width at half maximum value (FWHM) of 90 nm. In addition, there happens to be connecting wires among those spheres which is mentioned to have considerable importance although it is a minor detail. Also, it is claimed that disordered packing is more advantaged than ordered ones in terms of photonic properties. Another beetle they investigated is *Eudiagogus pulcher* which have crystalline structure formed of periodic sheets that includes hexagonal holes distributed with lattice constant of 450 nm. This sort of configuration gave beetle color spectrum centered at wavelength of 640 nm with FWHM of 100 nm, thus it looks like an orangish red.

2.2 Functional Surfaces

As nature offers plenty of environmental conditions, biological systems have evolved to cope and survive the difficulty of those conditions. What connects livings to the outside world is their surfaces and they are developed over the years to match survival necessities required by the reactive environment [56]. Natural systems have almost perfect surfaces among number of possibilities for which they have featured not only macro- but also micro- and even nano-sized structures. Functional surfaces that are produced as a way of adaptation to harsh natural forces exhibit variety of advanced features that can be integrated in our technological world. Most celebrated properties of those surfaces are superhydrophobicity, superhydrophilicity, superoleophobicity and wettability all of which are currently given very much attention and have already been used in wide applications such as self-cleaning window glasses and solar cells, drag reduction of underwater devices etc [57, 58, 59].

2.2.1 Review of Smart Surfaces

The study of biological designs and making derivations inspired by those functional structures to advance our technological devices or solve our scientific problems is known as the field of biomimicry [57]. Natural systems always provide significant insights that are not employed as a part of current advancements. It is not only concerned to integrate unique designs into our technology but manipulating them to further develop properties and to be used in a variety of applications are also established. From the point of functional surfaces, some analytical techniques have been found to investigate and characterize surfaces among each other. Those methods mainly includes contact angle and sliding angle.

Contact angle (CA) is the measure of angle at the location where liquid/air and liquid/solid interfaces meet and it provides a specification for tendency of liquid to spread along the surface, wettability [60, 61, 62]. As can be guessed, contact angle varies with ambient temperature and pressure apart from surface

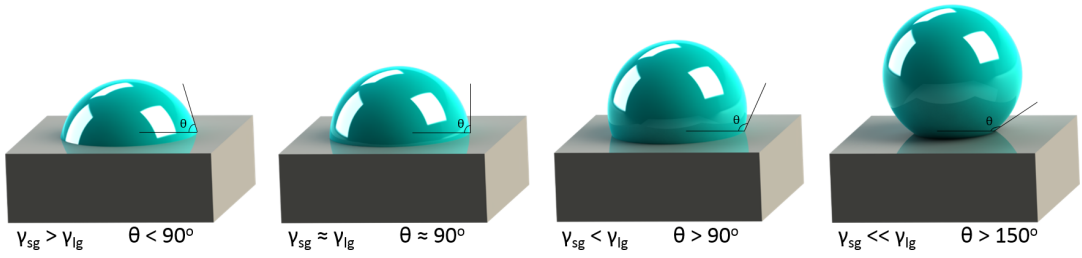

Figure 2.13: Contact angles according to different surface energy correlations.

structure which is its fundamental purpose of characterization. Thermodynamical mechanism explaining angle of measurement is based on surface energies among three phases: vapor, liquid and solid. Contact angle is simply related to surface energy difference between solid interfaces, and its cosine value with liquid/air interfacial energy gives that difference.

$$\gamma_{sg} - \gamma_{sl} = \gamma_{lg} \cos \theta_{ca} \qquad : \text{Young's equation} \tag{2.11}$$

It can be measured by drawing a tangential line to liquid surface where it intersects with touching point of the water. The angle between this line and the surface of the solid gives the contact angle. Therefore, contact angle can vary from 0° to 180° that can specify property of the surface to tempt to keep or get rid of the liquid.

In Fig 2.13 those cases are given as schematics. When surface energy between liquid/air phase is smaller than the surface energy between solid/air, water will face small vapour resistance which cannot prevent yielding. As solid/air surface energy increases water starts to stabilize thus leading to increase in contact angle.

Second analytical technique used as a measure of quality of the surface is sliding angle (SA) [63, 64]. It is the angle necessary to make liquid on surface starts to move, in other words as one side of the substrate is lifted liquid drop slides along the hydrophobic surface. Explicitly, this method is usually used to compare superhydrophobic surfaces because such structures can have high contact angle but sometimes do not respond well to inclined plane. In addition, contact angle on some surface may change as the drop moves from its originally intended location thus having higher sliding angle than the first point. If the sliding angle

is high for a surface then it means liquid sticks to surface which is not desired for self-cleaning applications since it leaves traces and does not roll off.

Using above mentioned analytical tools a surface can be characterized as hydrophobic, hydrophilic or oleophobic. Hydrophobicity is a physical property of molecules and surface that corresponds to repulsion of water. There are two important components on a surface that contribute to hydrophobicity, and they are surface architecture (roughness) and chemical composition [62, 65]. Structural roughness usually does not decide for surface to be hydrophobic, but it helps to increase the hydrophobicity to even higher degrees. The real mechanism defining hydrophobicity is chemical composition. If a surface has contact angle higher than 90^o it is ascribed as hydrophobic, and if its CA exceeds 150^o that makes the surface superhydrophobic. A molecule or a surface must have low enough surface energy to have hydrophobic property and this is decided merely by chemical structure. And they are further modified to obtain superhydrophobicity because no flat surface possesses such significant characteristics by itself. In other words, thermodynamically it is known from Young's equation that an unmodified surface cannot have CA higher than 120^o, therefore additional component must be added [62]. To have high contact angles surfaces are usually exposed to fluorination because -CF_3- component has the lowest surface energy [61]. For example, one of the most hydrophobic flat surface is polytetrafluoroethylene (PTFE), commercially known as teflon has CA of only 110^o which is comparably high for flat surface due to -CF_3- structure. However, for a modified surface with optimized roughness and chemical components CA can reach maximum value of 180^o. Budunoglu et. al. reported CA = 180^o on organically modified silica (ORMOSIL) aerogel coated glass substrate with SA smaller than 1^o [66]. In addition, superhydrophobic surfaces are required to have sliding angles lower than 10^o for self-cleaning purposes.

On the other hand, hydrophilicity is the opposite of hydrophobicity, i.e., it is the tendency of a molecule or surface to spread water. This feature is also ascribed depending on the contact angle. Values lower than 90^o is indication of hydrophilicity and smaller angles than 10^o is known as superhydrophilic. As in

the case of hydrophobicity, this feature is also upgraded with roughnesses utilizing spaces that have micro- and nano-sizes, beyond high chemical free energy of the surface [67, 68]. An example can be given for highly hydrophilic surface as titanium-dioxide (TiO_2) photocatalyst coated substrate [69]. Such structure almost does not exhibit any contact angle, it is very close to 0^o, therefore when water meets this kind of surface it runs off the edges very quickly. This functionality of a surface is also a possibility to be used as self-cleaning structure.

Oleophobicity is similar to hydrophobicity but here liquid material to be repelled is oil instead of water [70, 71]. Limitations to contact angles are also identical. However, this feature is more celebrated for surfaces that are originally hydrophilic, in other words if surface has CA¿90^o for oil in presence of water then with the help of this, oil drop residing on structure can be floated away with water supply. Property exists due to lower surface tensions of oil than water. This sort of feature can be used in environment where contamination form organic molecules is high. Such structures help systems to have low drag underwater, for example drag during turbulent flow can be reduced.

2.2.2 Multi-Functional Surfaces on Plants and Animals

Above-mentioned functional surface properties: hydrophobicity, hydrophilicity and oleophobicity have been investigated for a few decades, however they are being promoted to their limits with the help of the designs observed in biological systems. In most of the natural samples, roughness effect is more prominent than material properties. Roughness of the biological surfaces are mostly governed by micro- and nano-structures. Best functional surfaces usually include hierarchical roughness which includes two or three order roughness by utilizing nano-scaled levels on larger, micro-size structures.

One of the most studied natural topic for its functionality is surface of the Lotus leaf. Although it has been long known and observed for Lotus to have very high hydrophobicity thereby self-cleaning property, it had not been investigated until two decades ago. Barthlott *et. al.* reported first detailed investigation

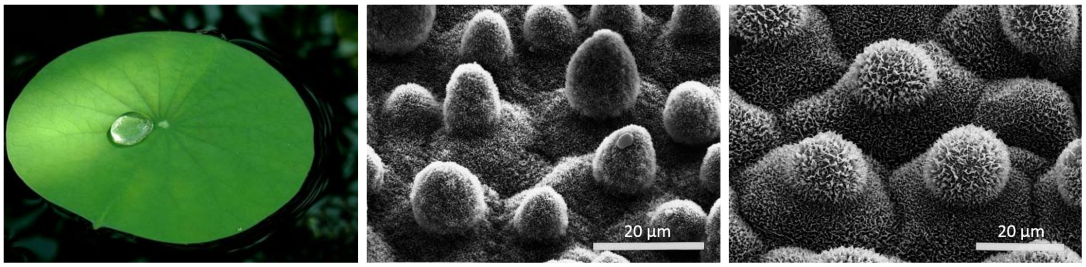

Figure 2.14: Microstructures on Lotus leaf are found to consist nano-pillars which promote hydrophobicity even further. Adopted from Ref. 72.

in 1997, and they showed that this leaf has contact angle around 161^o which is exceeded in some measurements. In addition, Lotus leaf is provided to roll the water droplet off in sliding angles smaller than 5^o, which is shown sometimes to be as small as 2^o.

According to first reports, microstructures and epicuticula wax considered to contribute to this type of hydrophobicity, however it was later demonstrated that nano-sized pillars exist on micro-sized papillae to promote hydrophobicity. This was also confirmed with theoretical calculations which have shown that leaf cannot be superhydrophobic without existence of nano-branches. Feng *et. al.* declared that Lotus leaf without nanostructures can at most reach 147^o, and further demonstrated, by simulations, contact angle of 160^o with nano-pillars. Fig 2.14 shows electron microscopy images and roughness scales, taken by atomic force microscopy, of Lotus leaf. Micro structures have diameters reported to range from 5 to 9 μm and they have nano-pillars with diameters averaged around 125 nm.

There are multiple examples to superhydrophobic surfaces that also show interesting properties. For example, in addition to lotus leaf, rice leaves are also observed to consist similar structures with micro- and nano-scale papillae [72, 73]. However, this surfaces also shown to possess anisotropic wettability that is known for materials to have different contact angles in different planes. In this case, rice leaves are superhydrophobic (CA $> 150°$) in one direction-parallel to the leaf edge but only hydrophobic (CA $< 150°$) in the other direction. Correspondingly, sliding angles also differ in two perpendicular direction, one is being below $5°$,

other is above 10°. An example from animal world is butterfly wing, they are not only colorful for their photonic crystal structures but also superhydrophobic.

As an example to hydrophilicity, pitcher plant is the most commonly known and investigated biological system [74]. Its ability does not directly include water contact, but insects that land inside of this plant experience slippery surface. Thus, they fall into a special liquid that serves to drown the insects and eventual digestion of them. Bohn *et. al.* reported effect behind the slippery mechanism as epicuticula wax and roughness. They commented that roughness can rise hydrophilicity as it promotes hydrophobicity depending on the chemical structure of the surface. In other words, surface exhibiting CA smaller than 90° without roughness can become superhydrophilic when roughness introduced. However, they do not declare any contact angle measurements on that surface.

On the other hand, oleophobicity is highly observed in natural samples that live underwater or contacts water occasionally [57]. Snail shells, fish surfaces and shark skins are particular examples. It was observed that although oil on snail shell makes contact angle of 10° when water is present oil does even attach to the surface. Fish scales are already known for their clean surfaces even in polluted water with oil. These natural systems's oleophobicity usually useful for self-cleaning purposes which serves to protect from biological contaminants. Shark skins have oleophobic surface that not only acts as self-cleaning structure but also assist for low adhesion thereby low drag underwater.

In the context of this thesis, we have also investigated surface structure of *Anas Platyrhynchos* species. It is demonstrated that neck feathers of Mallard duck are not only colorful with 2D photonic crystal, but they also exhibit superhydrophobic feature for self-cleaning purposes. We come to conclude from SEM images that there are three hierarchical roughness levels contributing to superhydrophobicity(Fig 2.15). First order is the gaps present among the barbule arrays that extends from main feather. Second order roughness is observed to be the interlocking steps between longitudinal segments in each barbule cluster. As the final hierarchical components is the nanoscale roughness on the surface of each barbule which looks like bumpy structure.

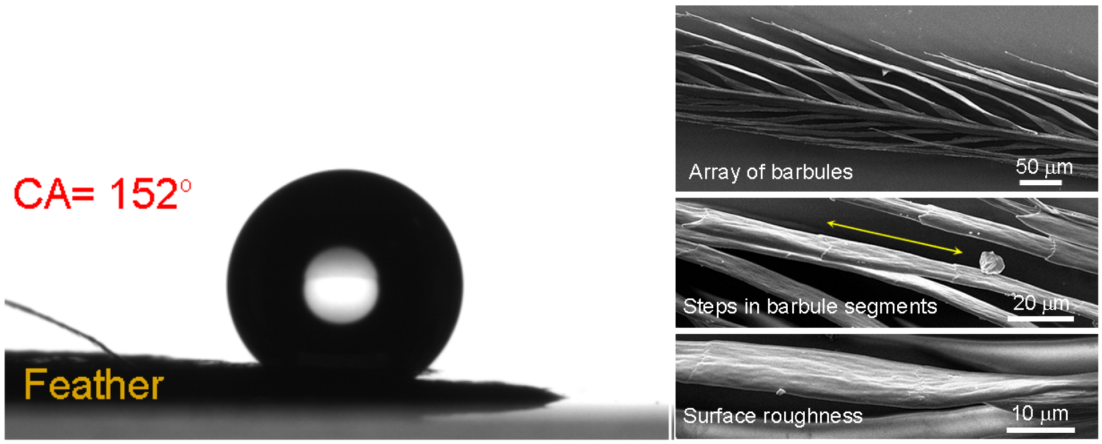

Figure 2.15: Feathers are found to possess (besides coloration), self-cleaning property which is considered to be emphasized by hierarchical roughness.

Chapter 3

Fiber Design and Fabrication

Production of nanowires and fibers has been a great challenge for scientists. However, association of fabricated materials to one system has been more formidable problem in the way of technological developments [75, 76, 77]. Although there are plenty of techniques both top-down and bottom-up that result with required properties in size, material and alignment, most of them lack at least one essential credential without which problem is not exactly solved. Most reports for new devices employ nanowires that are outcomes of bottom-up chemical synthesis and these nanowires have shown very significant progress in terms of size, crystal structure and material composition, however they are unsuitable for mass production and usually used for demonstration of desired properties or potential applications [78, 79, 80]. Some suggests production of nanoscale parts directly on the chip whose integration to a larger apparatus is straightforward, but these methods still need their time to reach maturity so that they can sufficiently satisfy technological demands [81, 82]. For top-down production methods, lithography and electrospining are the most used ones, however photolithography cannot go beyond diffraction limit and electrospining has very serious alignment issues despite of which fact they are still convenient for variety of applications [83, 84]. For the production of fibers that are milestones of this thesis, we utilized recently discovered iterative size reduction method that overcomes above-mentioned problems [85].

3.1 Iterative Size Reduction Method

Fiber drawing has been a well-established production technique to achieve very uniform and long fibers [86, 87]. Through this process cross-section of a material is reduced up to 300 folds by applying force while heating. It is usually used to draw silica tubes from macro-scale to micro-scale in a single step using optimized parameters. Currently, produced silica fibers are commonly in use for communication, sensors etc. purposes. Mostly, single set of glasses are drawn at specific temperatures and other fabrication parameters, because each type of material has a unique glass transition temperature. However, drawing fibers with composite materials requires components to have close transition temperatures and thermoelastic properties. It is important for them to reach to a soft state where each of them will reduce in size without breaking into pieces.

In iterative size reduction (ISR) technique, materials can be drawn down to nano-scale in an arrays of hexagonally ordered millions of wires. The process utilizes thermally compatible material and polymer jacket to be drawn multiple times iteratively. First starting point for iterative size reduction is macroscopic material rod which is turned into nanowires in the end of the process. Then thermally compatible polymer jacket including this rod inside, which is called preform, is established for drawing purposes. Preform is heated to a temperature level where both materials exceed their glass transition temperature and become soft enough to reduce in cross-section under application of an adequately large force. This step is quite similar to commonly known regular fiber drawing method and only significance is that it includes composite materials. Optimized sizes in this technique of the first preform and first step fibers are ranging from 25 mm to 35 mm and from 100 μm to 1 mm, respectively.

Most prominent side of ISR is utilization of first step fibers for another drawing step to obtain another dimensional reduction thereby micro-scale fibers. Fibers obtained after first drawing are cut into smaller frames and bundled up together and placed into a hollow preform again prepared from thermally compatible material, usually polymer. As energetically favoured state, placed fibers with uniform sizes homogeneously distribute themselves radially inside the hollow core. After

thermal drawing process takes place, indefinitely long fibers that include hexagonally arranged microwires are acquired. Same procedure as in step two can be employed to further obtain nanowires as a consequence of third step. In this last step, fibers from second step which already include number of micro wires are inserted into another hollow preform, thus including as many times more wires in a preform. In other words, new preform contains plenty of fibers that include that much of more wires. For example, if filling factor for a hollow preform with 10 mm hole is 500 fibers, then third preform has around $500 \times 500 = 250.000$ wires. Parameters and drawing procedure similar to second step is followed to produce third step fibers with hexagonally distributed microfibers that have hexagonally and uniformly aligned nanowires. As mentioned above, at each step reduction factor (RF), that is the ratio of final diameter to initial diameter, can change from 25 to 300, and simple consideration of 100 fold reduction at each step gives $\mathrm{RF} = 100^3 = 10^6$, thereby 10 mm rod in the beginning scales down to 10 nm at the end of the fabrication. Drawing schematics and fabricated fibers can be seen in Fig 3.1.

Fibers concerned in this thesis are also produced with this technique. For drawing procedures there is a home-built fiber tower that consist multiple components each of which serve to set different fabrication parameters (Fig 3.2). Fundamental part for fiber drawing is the furnace which contains two heating compartment, top zone and bottom zone. Bottom zone heats the preform to desired temperature which is slightly above the highest glass transition temperature of the materials. This value is entered directly with user interface platform, and according to this value program sets the top zone temperature to a rate which pre-heats the upper section of the preform to be drawn in oncoming times. Evidently, preform is not completely placed into the heating zone and it is hold with a stage that can move in three dimension: X, Y, and Z (Z direction coincides with vertical dimension of the preform). X and Y positions of the preform are aligned before drawing starts so that preform is radially kept at the same distance away from the furnace surface. On the other hand, Z parameter is not set in the beginning and as soon as drawing starts it is set to a speed (feeding speed) by which amount preform moves downward so that drawn places are

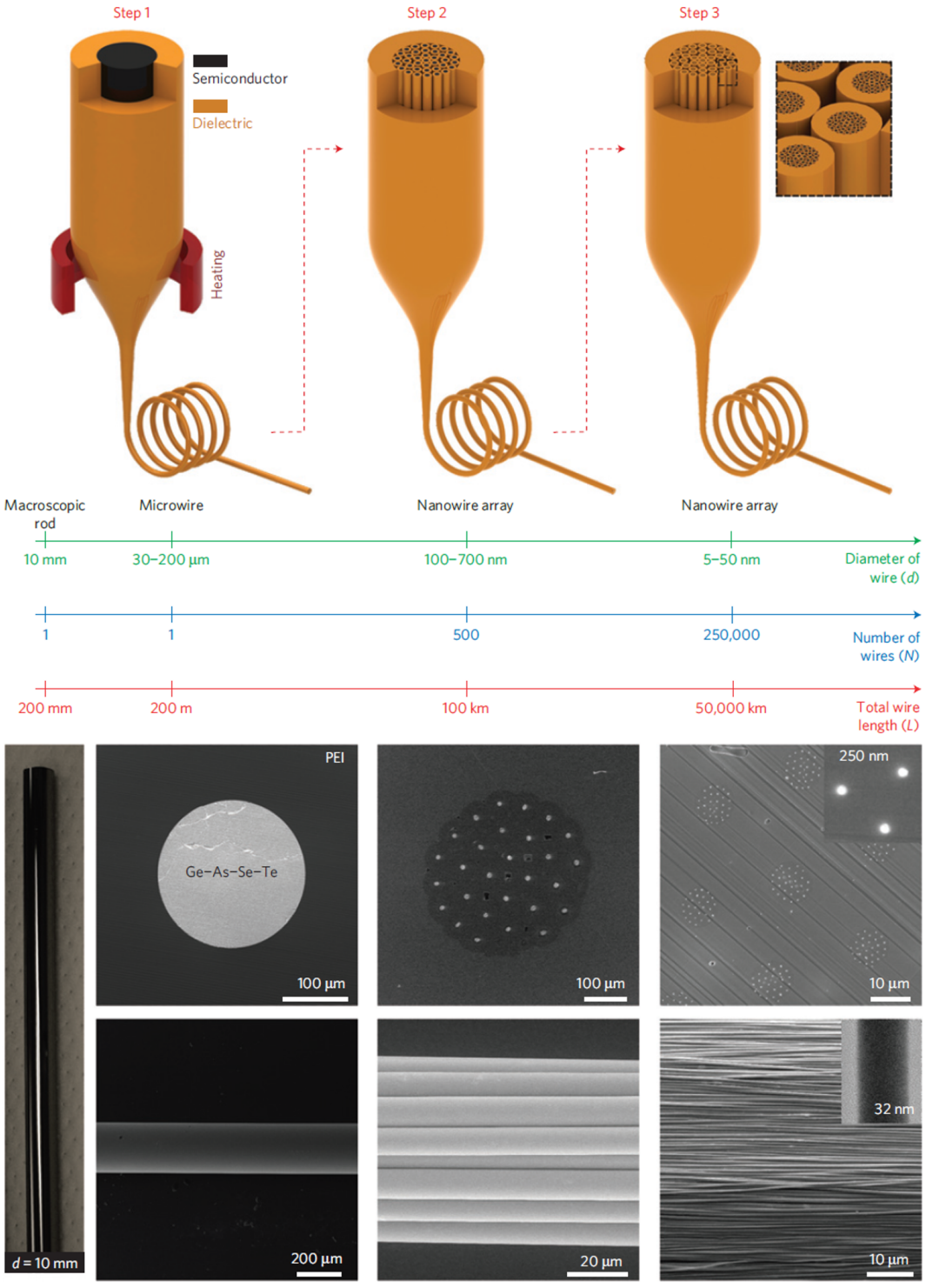

Figure 3.1: Schematic for iterative drawing procedure is shown. Resulting fiber cross-section and longitudinal SEM images are given. This technique helps to fabricate very long nanowires in desired orientation. Adopted from Ref. 85.

constantly compensated with pre-heated regions. As significant force required to start drawing, a small weight is attached to down side of the preform through which process is initialized after preform is heated to set temperature. Incoming fiber goes through a thickness measurement system that constantly measures and monitors thickness of the incoming fiber. After that fiber strolls tangentially to a series of pulleys one of which measures the tension of the drawn fibers since they are actually drawn with capstan at the bottom of the tower. Depending on the tension and thickness, capstan speed, feeding speed and temperature values can be arranged to optimize values or sustain homogeneity.

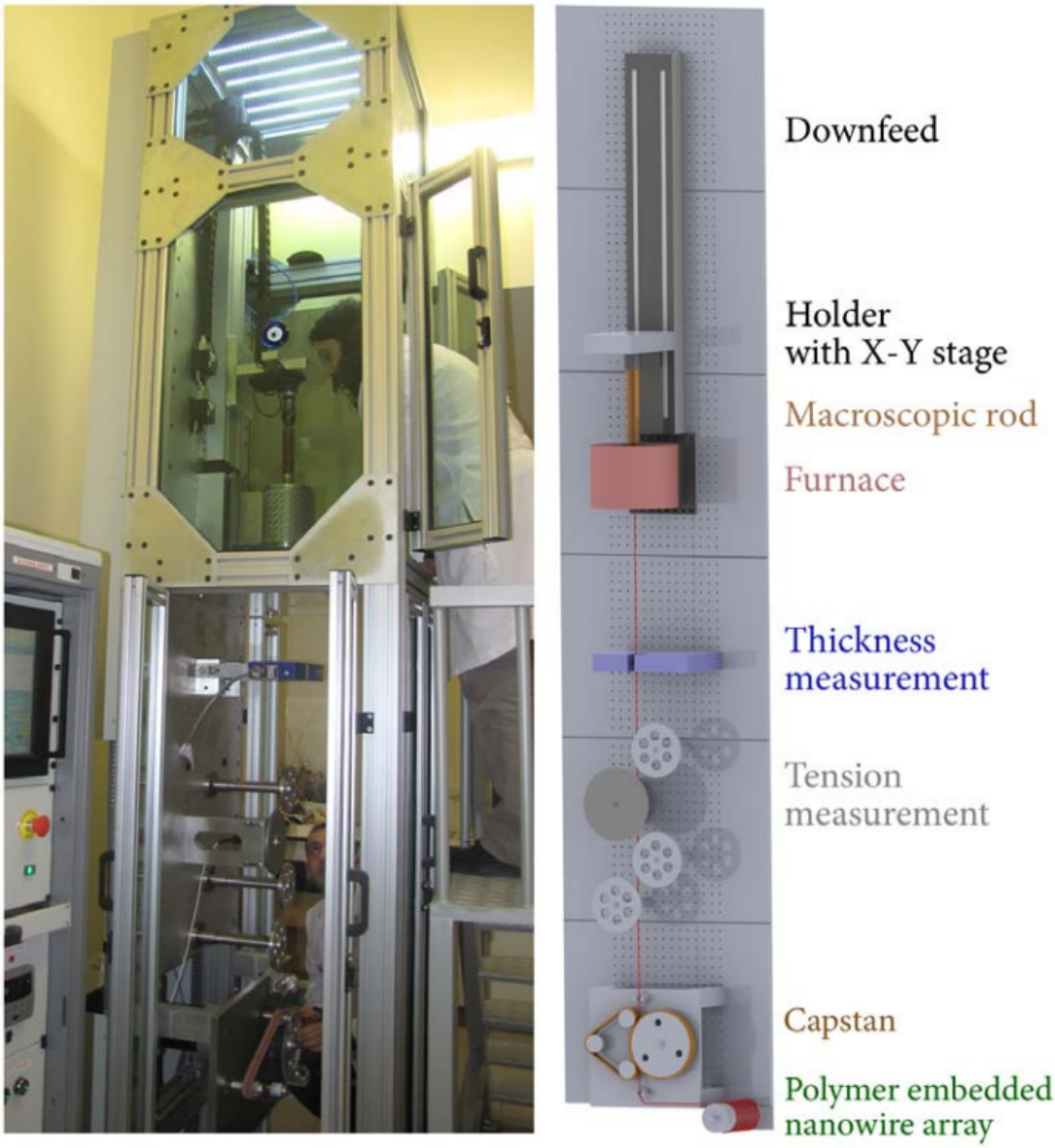

Figure 3.2: Home-built fiber tower used for iterative size reduction.

3.2 Material Characterization and Preform Preparation

Generally, glass semiconductors are drawn to form uniformly distributed array of nanowires because crystalline materials come as pieces inside the protective jacket. On the other hand, protective jackets are always made from polymers since they do not get viscous and spill as glassy materials. In addition, outer shell helps to create lattice arrangement in the further steps and keeps glass wires touching each other. To form two-dimensional photonic crystal fibers we considered using only polymer materials. There are multiple reasons for such selection.

First of all, duck's plumage is made out of polymer materials: melanin and keratin. These materials have refractive indices that are particularly close to each other and small enough to function at optical frequencies, 2.0 and 1.56 respectively. In our production, we had to use two materials that are compatible optically, therefore we decided to choose polymer materials since they have small refractive indices and it would be hard to find and manipulate two glass materials with low refractive indices. Secondly, polymer materials not only have low refractive indices but their indices sustain their values with minimal errors throughout the visible spectrum. Last but not least, polymer materials are usually thermally compatible and easy to draw since they do not go into small pieces like glass materials even if temperature is considerably higher than their glass transition temperature.

Table 3.1: Polymer materials

Materials	Drawing Temperature	Refractive index	Specific Gravity
PVDF	180 °C	1.41	1.78
PC	220 °C	1.58	1.21
PES	226 °C	1.65	1.37
PEI	223 °C	1.67	1.27

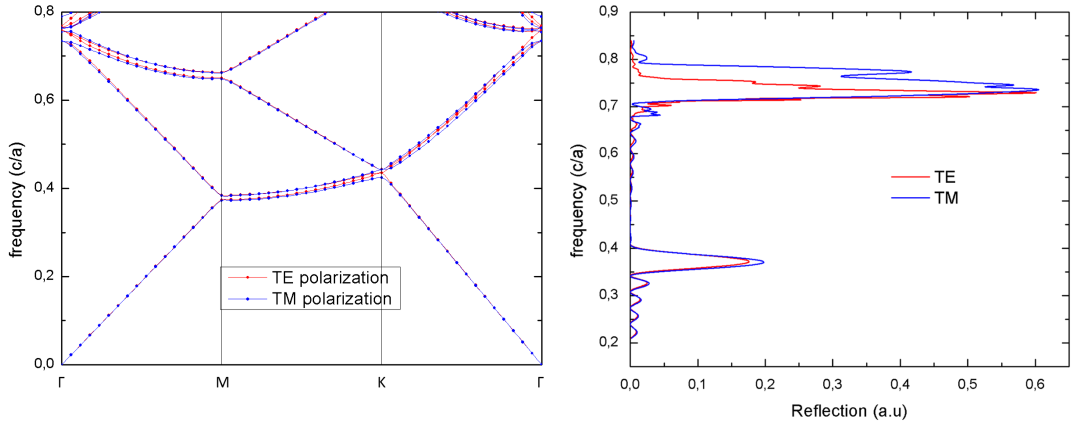

Figure 3.3: Band diagram and reflection simulations carried out before drawing procedure to estimate required rod sizes.

In Table 3.1, different polymers with distinct properties are given. From these, we are supposed to select two materials that have comparatively large refractive index difference. Therefore, PES and PEI cannot be selected as corresponding pair. Either PVDF/PC pair, or one of the PC(PVDF)/PES(PEI) pairs must be concluded. Refractive index difference of materials in mallard feathers is $\Delta n = 0.44$. Even this value is particularly high, simulations (Fig 2.11) made for photonic crystal structure in the barbules suggest that difference should not be very small, otherwise bandgap might become pinched causing prevention of reflection. This argument implies that we should select PVDF/PC pair, and we selected those two, however there are two other motives that reinforce accuracy of our selection. One of the two considerations is that PVDF has fluorinated residues and as mentioned in Chapter 2 fluorinated compounds are known to promote hydrophobicity. Such property could help us to manifest superhydrophobic feature for our produced 2D photonic crystal fibers. Another reason to approve PVDF/PC polymers is that PC, unlike any other polymer, can be removed easily by peeling off from the surface of PVDF, and this will facilitate fabrication procedure since it is required to remove PC jacket after first step. From all of these factors, PVDF/PC polymers are deduced to be most suitable pair.

To ensure that selected polymers will result with small bandgap around 500 nm wavelength (green color), we run simulations both to see significant reflection

and band diagram. Fig 3.3 demonstrates the simulation results that has parameters of r/a = 0.433, n_{PC} = 1.58 and n_{PVDF} = 1.41 as fixed values. Simulation for band diagram is carried out in MIT Photonic Bands (MPB) software, and reflection spectra is calculated via FDTD solutions by Lumerical program. As expected, results show proper band gap and reflection values for chosen polymer pair. It should also be noted that iridescence is still emphasized, such that, band gap is small enough not to combine multiple wavelengths at certain direction of view. From the points of frequency we can infer the lattice values to which rods are supposed to scaled down. Using eqn 2.10, we get

$$a = f\lambda \qquad a \approx 0.400 \times 500 = 200 \text{ nm}$$

Thus lattice constant must be around 200 and thereby radius of each rod is supposed to be 200×0.433 ≈ 86 nm. Final points give us insight about ratios that we should use while preparing preforms.

Before starting to arrange first step preform, we have considered the second step because in the second step we insert fibers from first step but there still remains space among them since cylindrical fibers cannot fit perfectly without leaving some space. This condition makes the distance among rods shorten since outer shell fills the empty spaces while drawing and decrease in thickness. Reduction in lattice might look negligible but it is not that small to ignore. Therefore, to avoid such circumstance we planned to increase thickness of the shell layer in the first step. With this in mind, we considered to prepare a preform which consists 10 mm PC core and total 12 mm with PVDF shell, *i.e.* 2 mm thick PVDF layer, and total preform with outer protective jacket (PC) arranged to be 20 mm in diameter so that we can still control fibers after drawing.

Preforms are prepared by rolling films around either glass rod directly or teflon tubes. Here, we first needed a PC rod and for this we rolled PC polymer films around thin (4 mm) teflon tube to form a huge (30 mm in diameter) preform. Then this preform is consolidated using a home-built consolidator device (Fig 3.4a). Consolidator heats the preform uniformly to a state where rolled films combine to become fused under vacuum environment with pressure of 10^{-3} Torr.

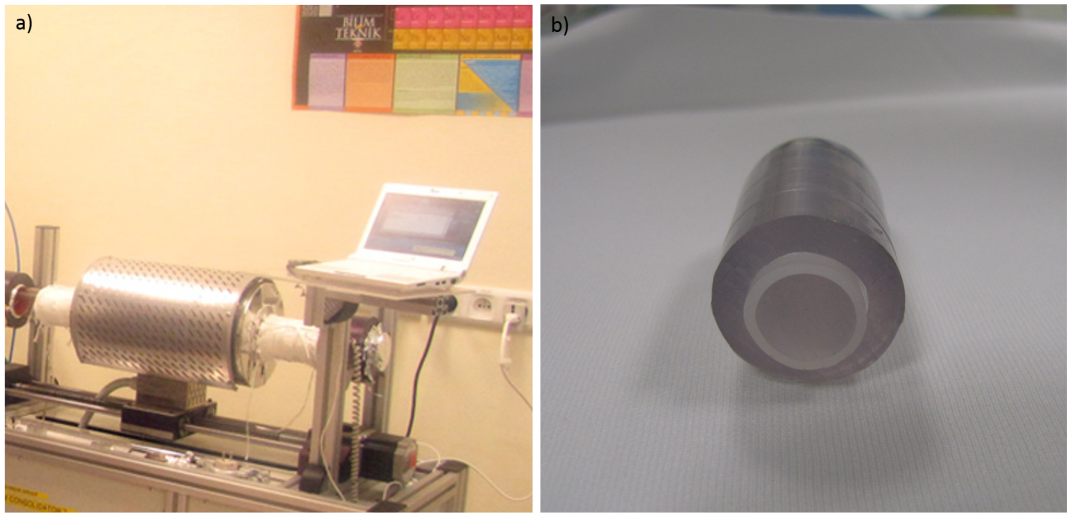

Figure 3.4: Home-built consolidator and prepared first step preform.

For PC, consolidation process includes 2 hours waiting in 140 °C and then ramping by 2 °C/min to 185 °C where it is hold for 10 minutes to fully consolidate. Then, this preform is divided into four equal pieces through its cross-section. One of this pieces is smoothed to become 10 mm rod using turning machine. The reason to take this route is that any preform rolled on a teflon tube results with hollow core inside and this might cause shift or defects in the color of final 2D photonic crystal. After this process, 10 mm PC rod is simply rolled with 2 mm PVDF shell and 8 mm final PC jacket, successively. Then whole preform is consolidated at temperatures similar to above-mentioned consolidation procedure. Fig 3.4b shows the schematics for first step preform preparation, and final preform.

First step fibers were drawn at temperature of 224 °C to final thicknesses around 600 μm which means reduction factor of 30. Fig 3.5 shows the first step fibers after fabrication and SEM images of cross section. As it appears and expected, fibers preserved their initial aspect ratio throughout the drawing process thus concluding with high regularity. First step fibers were well-established and, as it was intended from matter of choice, PC jacket around the fibers were easily removed by simply peeling off, after which fibers were ready for second step.

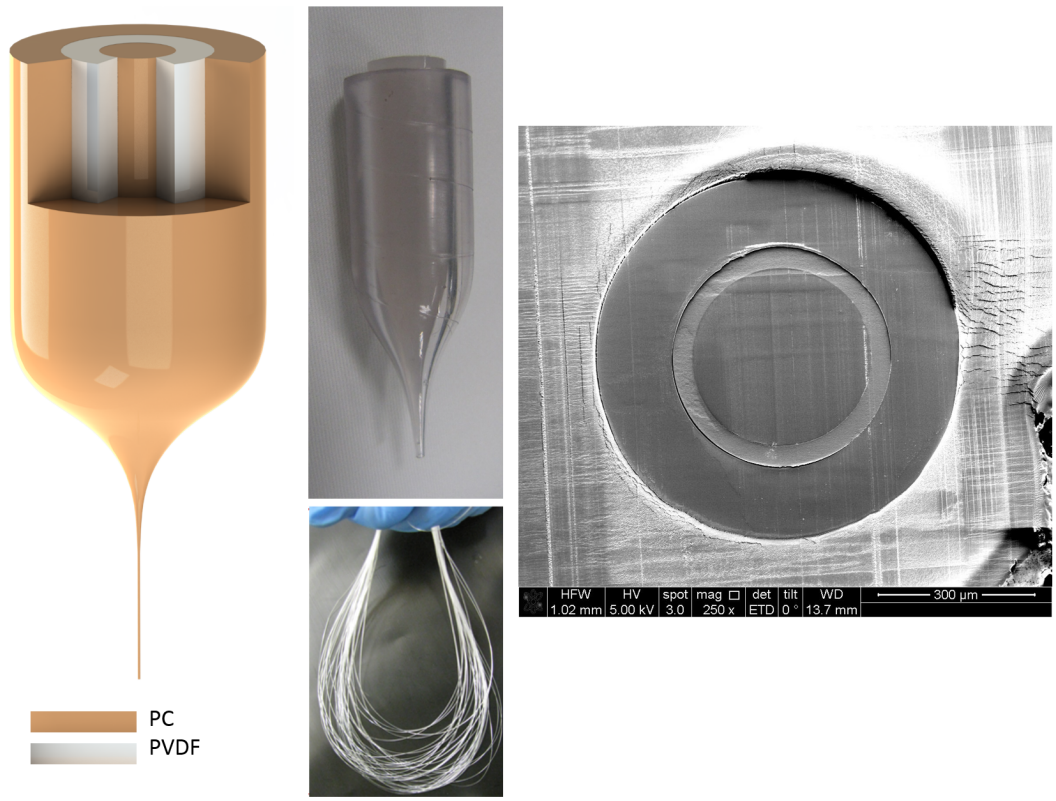

Figure 3.5: Schematic for first step drawn preform and real preform are given. As it is clearly observed from SEM images, fibers preserved their cross-sectional ratio throughout the drawing process.

3.3 Design and Fabrication of Novel Preforms and Fibers

In the second step, we needed to bundle up these fibers in such a way that they do not only form hexagonal lattice arrangement but also have large surface area to reflect light. For this reason, we considered to form up a rectangular shaped preform, which should have smooth inner surface. Usually, preforms are rolled around a tube for two reasons first of which is to have circular hollow core and second if it cannot be removed by hand, glass tubes are easily dissolved in hydrofluoric (HF) acid solution. Dissolving method is generally tried to be avoided because it takes some time for tube to dissolve. However, since surface are of tube is much larger than rod, they take much less time to corrode. For our purpose, we rolled the preform around a simple microscope slide. As expected, films were unable to cover smoothly the glass, but after consolidation they softened and covered the glass substrate completely. Afterwards, this preform dipped into 48% HF solution and left there for 2 days even after which glass merely half dissolved. Then we scratched glass throughout the preform to increase the surface area and help dissolved glass from top fall off through. After 2 more days in HF solution, glass was weekend as a structure, so it broke easily and came off leaving a PC preform with highly uniform and smooth inner surface. Around 500 first step fibers are inserted inside this preform. We did not worry about hexagonal distribution because it is energetically most favoured state for fibers to form. Fig 3.6 shows the preform and fibers in it. This sort of preform is novel due to its high aspect ratio cross-section and fully polymeric composition.

First step fibers had core diameter only around 350 μm and it should scaled down with a reduction factor of 2000. However, this could not be accomplished in a single step, therefore we thinned down second step preform by only RF = 10. The reason for this was to have hexagonally distributed fibers concatenate in this step, and to observe results on large scale before we continue to drawing process. Fig 3.6 demonstrate the results after second step drawing. At a first glance, it might seem like hexagonal distribution is not emphasized, but careful investigation gives solid results. It should also be noted that few defects and

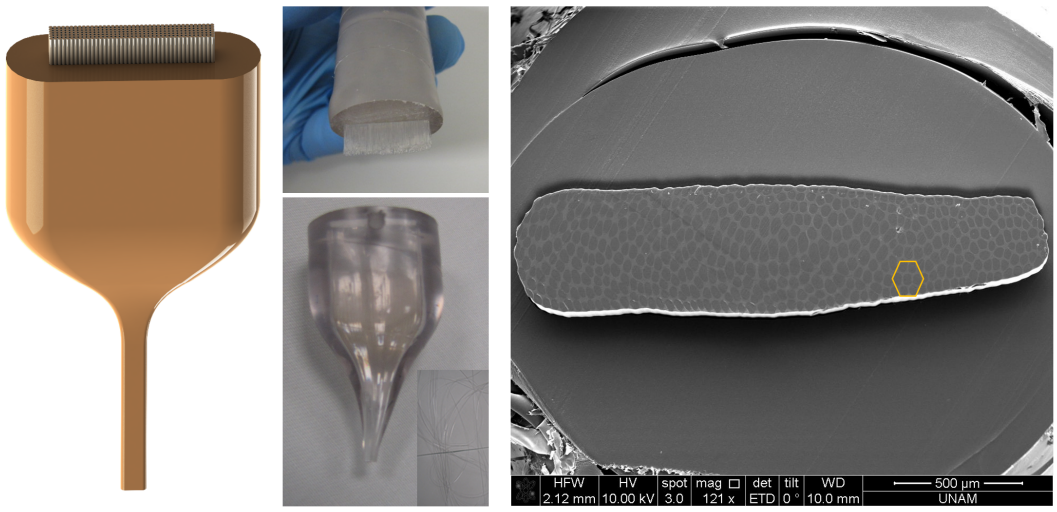

Figure 3.6: Real and schematic second step preform are given. Cross-section of second step possess hexagonally distributed micro-scale rods.

derangements at particular points along the lattice is not expected to violate the integrity of overall photonic crystal configuration. This claim will be proven at the end of all steps.

3.3.1 2D Photonic Crystal Fibers

After accomplishing second step fibers without any corruption, it was needed to scale those fibers down once more with a reduction factor of around 200 so as to obtain two-dimensional photonic crystal fibers that contains nano-scale elements, thus functions at optical frequencies. However, there were still necessary requirements to be met for successful fabrication of such fibers. As it has been intended and concluded up to this point, second step fibers have unusual cross-sectional geometry that is rectangular shape. It must also be contemplated for fibers to conserve this aspect throughout the final drawing step. To meet the same circumstances, a third step preform similar to one used for the second step is prepared, i.e., preform with smooth rectangular hollow core. By this means, fibers can be prevented from any derangements or any disintegrations that can be caused from circular core. On the other hand, a single fiber still cannot

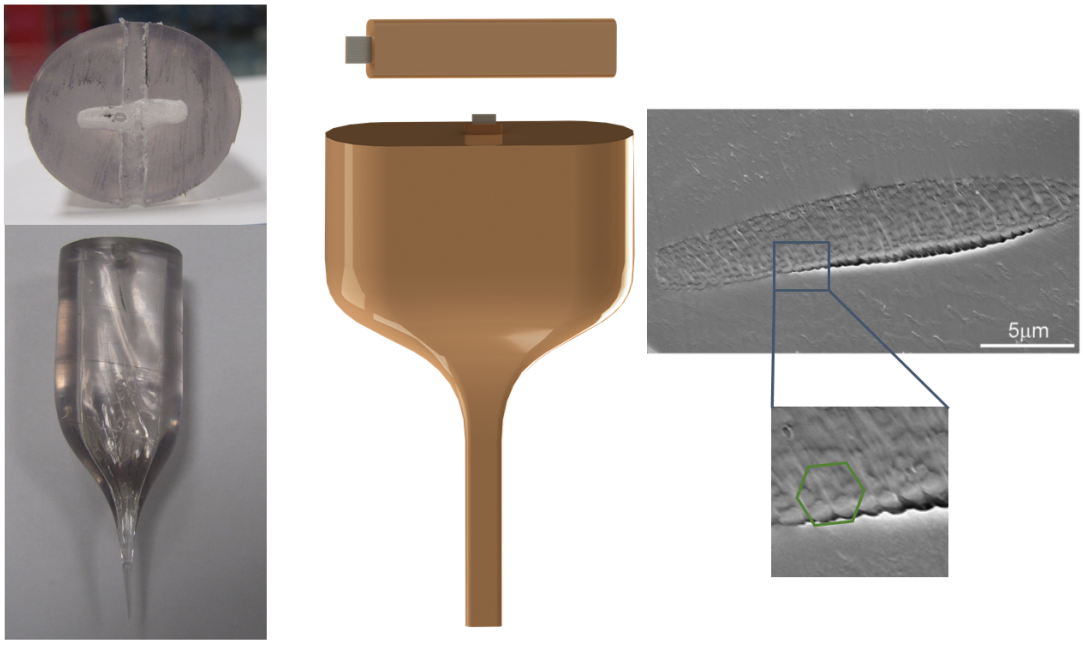

Figure 3.7: Only single fiber is inserted into third step preform since it is just aimed to decrease its overall size.

completely fit to this hollow core, therefore we considered inserting additional polycarbonate fibers, which are made of the same material with the preform, near the fundamental fiber. In this wise, fiber can fit inside the preform perfectly without having any degree of freedom which may cause distress while drawing. Fig 3.7 demonstrates the prepared preform.

Through handling all problems, third step preform was meticulously prepared and ready to draw. However, since it is determined to reduce by factor of 200 in this step and last fibers will include nanoscale elements, parameters and procedure in this step must constantly be checked so as to anticipate and response accordingly to any change while drawing. Mistakes committed in this step can result with lattice corruption which could lead segments with ruined color throughout the fibers which are purposed to possess single color for a long range. For this reason, fibers must be scaled down easily, in other words reduction factor must be increased by time in this last step at the end of which reduction could smoothly reach 200-fold. Considering all of this, third step fibers were drawn successfully to obtain hexagonally distributed nano-size rods forming 2D photonic crystal fibers.

Fig 3.7 shows the cross-sectional electron microscope image of the obtained fibers.

Apparently, those fibers preserved their rectangular cross-section thanks to taken precautions both at preparation of final preform and while drawing procedure. SEM images are not completely clear due to low refractive index difference among both materials, PC and PVDF. However, it is clearly visible that rods are arranged in hexagonal formation. Close captioning to certain sections provides further support to this claim (Fig 3.7). In addition to that, it should also be noted that deviation of diameters of rods is considerably negligible by which it is meant that they will not affect overall color in a manner that reflected spectrum will be mixture of several wavelength.

Chapter 4

Fiber Characterization

From the materials point of view, drawn fibers are required to have two properties. First of these was hexagonal distribution of the nano-scale rods which are also embedded in a polymer matrix that is constructed from distinct polymer. This was achieved throughout the all drawing procedures by careful considerations and calculations. The other feature was surface roughness along the long edge of the rectangular cross-section. Since first step fibers were circular and they were directly placed in a rectangular core preform, they were expected to preserve such morphology on the edge although their shell material would combine inside the matrix. Electron microscope images suggest that there are cambered structure on the surface of the fibers.

Each of these material requirements were necessary to exhibit corresponding effects that will characterize fibers. Those effects, as this thesis concerns, are optical properties and hydrophobic properties. Fibers characterization are concluded using fundamental setups. In this chapter, employed setups and results from bio-inspired fibers are thoroughly investigated and explained.

4.1 2D Photonic Crystal Fibers For Bio-Mimicry of Anas Platyrhynchos L.

Inspiration for produced 2D photonic crystal fibers was Anas Platyrhynchos, commonly known as mallard duck or green-headed duck. First investigations were done to demonstrate success rate of achieving mimicry of such unique feathers. As explained in the second chapter, those feathers show incredible green coloration due to 2D photonic crystal effects. In addition to bright colors, situated photonic crystals also cause iridescence on segments of the feathers. In real life, iridescence is observed as disappearance of color as angle of view is changed from direct to sight from an angle. However, more significant proof to iridescence is the color shift or more precisely, shift in the reflected wavelength. Feathers of investigated duck have shown such iridescence and through fabrication of 2D photonic crystal fibers, this property is also expected to be mimicked to some degree.

Beyond photonic crystal effect, colorful feathers include rough surface and hierarchical roughness effects exist thanks to two components: interior growing mechanism of the feather and agglomeration due to natural side to side development of the barbules. Surface roughness aimed to be accomplished on fibers to mimic this effect. Through fabrication technique it also seems to be possible to acquire hierarchy among fibers not to only imitate hydrophobic effect but also promote it to a superhydrophobic degree and more.

4.1.1 Optical Characterization of Bio-inspired Fibers

Produced fibers had total sizes around 15-20 μm, and as it can be inferred, they do not exhibit visible color to naked eye, they are even hardly visible. Therefore, to provide color and iridescence, optical microscope is utilized. However, to further characterize reflection from 2D photonic crystal fibers, an optical setup is established (Fig 4.1). In terms of configuration and employment, this setup is very simple since optical microscope is the main part. A spectrometer is connected to microscope using an optical fiber which collects direct image(light) from display

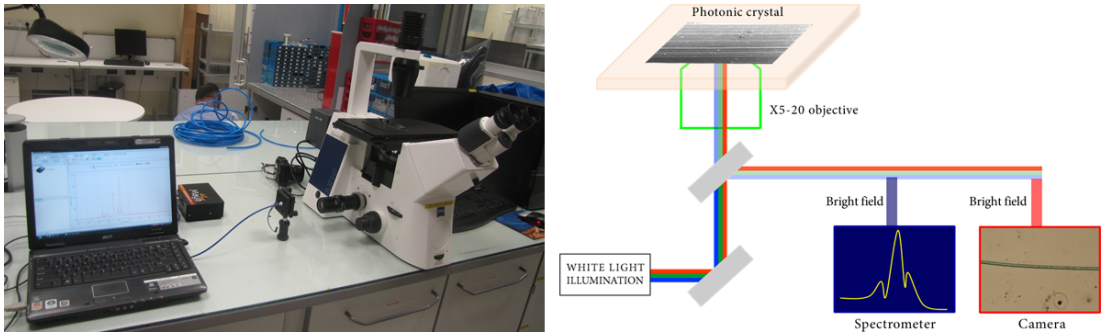

Figure 4.1: Photograph of optical setup. Mechanism used can be understood from schematics.

output part. Spectra with wavelengths in the visible range is accumulated from incoming light and directly monitored through live-feed on computer screen. By this means, apparent color in the microscope can directly be measured without performing any additional preparation.

Third step fibers were embedded at the core of a polycarbonate matrix that was imposed to protect fiber in the third step drawing. However, to take clear measurements and benefit from full effect of two-dimensional photonic crystals, it was necessary to dispose the outer polycarbonate. For this, we used an organic, chemical element known as dichloromethane (DCM) that has empirical formula of CH_2Cl_2. This chemical compound is widely known to dissolve polymeric materials, and we have tested to further check results. Apparently, our produced fibers have a crucial composition to survive from corrosion by this chemical. Our experiments show that this chemical responds to each polymer differently and etches them at different rates. Critical part in our case is that speed of etching PVDF is much more slower than PC, this means that we can safely etch polycarbonate outer shell and obtain clear, undistorted 2D photonic crystal fibers thanks to matrix material, PVDF. However, it is very important that we completely clean the outermost PC material before we take any measurements because of the fact that it can lead to color shift and disturbance due to thin-film interference effect. Therefore, to make sure complete decomposition we held our fibers longer than necessary time for PC to be etched. Although this induced some corrosion on the surface of the PVDF shell, it did not get into the fiber and cause damage to rods.

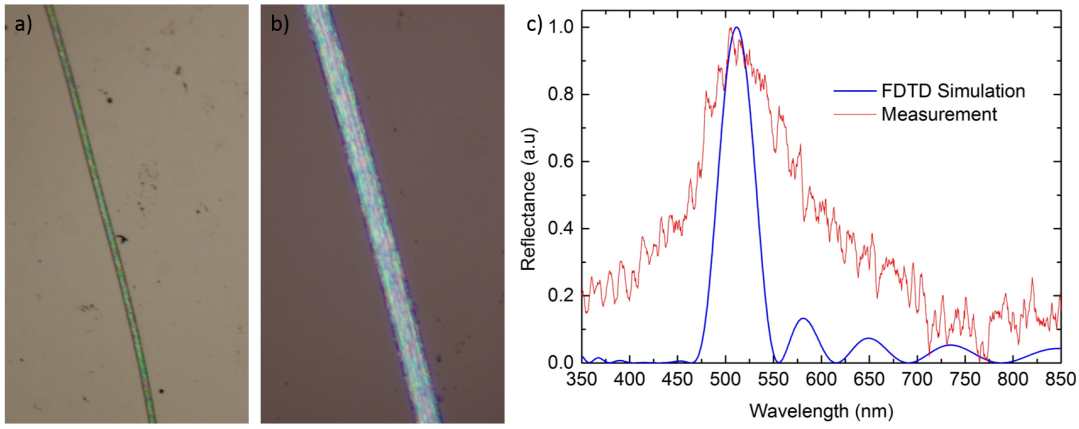

Figure 4.2: Green fibers show iridescent behaviour under higher magnification and the idea of matching between measurement and simulation further approves coloration due to photonic crystal effect.

It is noteworthy to say that fiber geometry has very high aspect ratio (1:15), therefore it is physically favoured for it to lean on larger side. Besides, since fibers are very long we can see if it has turned to different side. Considering this, fabricated fibers are carefully etched on microscope slides and are inserted into microscope to see color effects. As can be seen from Fig 4.2a, etched fibers are exceptionally green. It can also be observed that there are spots where different colors are produced such as red or yellow, however those are negligibly small segments comparing to large area of the fiber, therefore overall color is sufficiently dominant to reflect only green wavelength(s). To ensure produce color is due to photonic crystal effect, we switch microscope lens to higher magnification by which iridescence is expected to be observed. Fig 4.2b shows the same fiber with higher magnification, color shift to blue is clear when compared to previous image. This magnification also increases influence of the defects, spots with different colors are more visible, but the main color is still distinctively dominant.

Before we begin fabrication, we simulated results from 2D photonic crystals that was going to be fabricated. Here, we also compare measurements from given fibers. Fig 4.2c shows the great match between simulation and measurement, which are both normalized values of arbitrary units. This result manifests the superiority of the fabrication technique in mimicking the investigated photonic crystal structure. Also, success of the fabrication is clearly expressed.

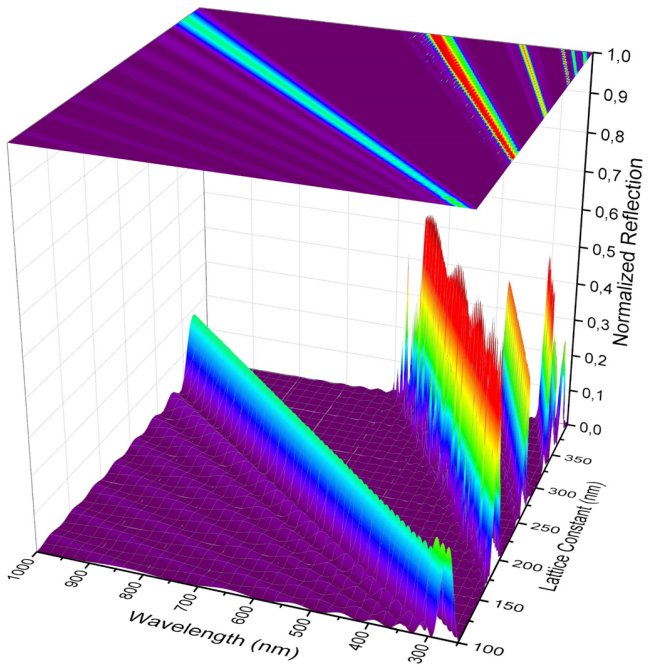

Figure 4.3: Adjusting to different lattice constants any wavelength can be reflected by 2D photonic crystal.

Calculation of band diagram of two-dimensional photonic crystals only necessitates dielectric constants and radius to lattice ratio. From this, it can be explicitly deduced that same photonic crystal configuration at larger scale will result with same band diagram. What makes the photonic crystal function at optical scale is the lattice constant, in other words, as equation 2.8 suggest color is directly dependent on the lattice constant. By taking this advantage, we realized that our fabricated fibers span a wide range in terms of lattice constants because we had drawn fibers by slowly reducing the overall size. To find corresponding colors regarding lattice constants, we produced a map (Fig 4.3) that will allow us to choose necessary fibers responsible for each color and also provide further theoretical support for observation of different colors. In this map, each peaked modes correspond the different bandgaps. We are interested and already produced color from the fundamental mode that is located along the diagonal of the map.

Considering lattice constants corresponding to main colors in the visible spectrum, we found and etched differently sized fibers to obtain full spectrum. As it

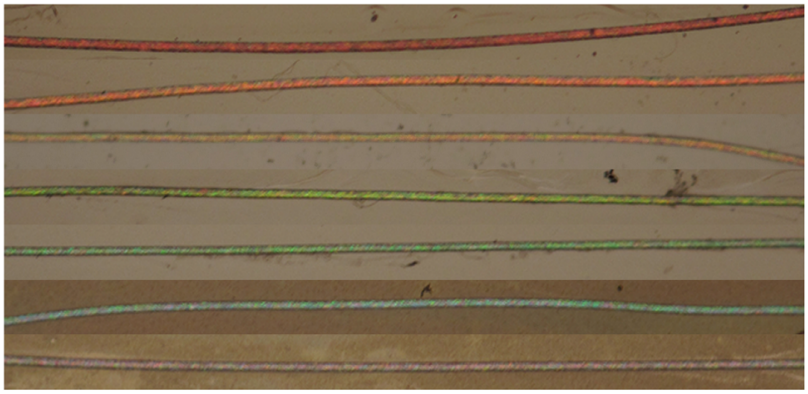

Figure 4.4: Using map řefcolormap for producing different wavelengths, colors of visible spectrum are produced.

can be seen in Fig 4.4, fibers that reflect all the main colors are obtained. All of these fibers were already produced in the final step of the fabrication. Considering this fact, excellence of the fabrication method on production of such specialized fibers emerges once more.

This result also emphasizes that fibers do not have to reflect only colors of the visible spectrum, they can also reflect different wavelengths depending on the lattice constant. Reminding once again, in the third step, we already produced fibers that span sizes of wide range, i.e., lattice constants change from a few microns to hundreds of nanometers. Therefore, fibers that reflect wavelength near infrared are already obtained and depending on the requirement photonic crystal fibers reflecting at frequencies from THz to GHz region can easily be produced.

Another compelling feature of fabricated fibers is their constitutionally contained materials. As it was intended to fully mimic the natural samples, we have especially selected polymer materials. These materials are particularly important for their close refractive indices to natural ones, and their nonhazardous structure. Additionally, as it is a fact for most of the polymers, at small scales they are easy to manipulate because of weak and soft structures as a course of their natures. We also utilized this knowledge to taper fibers and show tunable

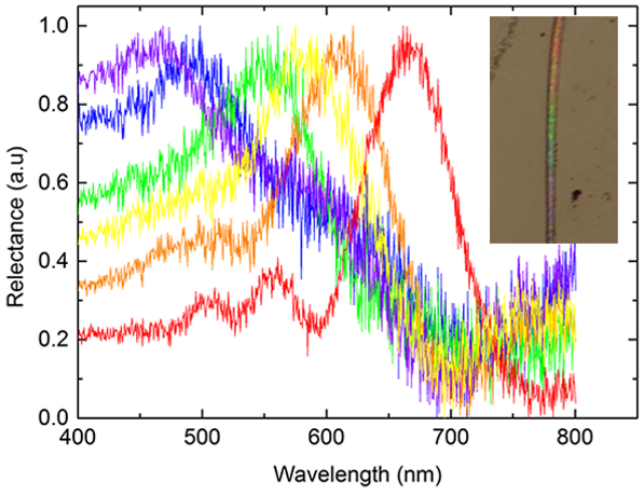

Figure 4.5: Single fiber can be tapered in a segment as small as 1 mm to reflect all visible spectrum.

property of produced fibers. As mentioned above, two-dimensional photonic crystals with same radius to lattice ratios and same materials will produce exactly same band diagrams, and their color can only change depending on their lattice constant. Therefore, if we take thick fiber that reflects wavelengths higher than visible spectrum, tapering it will construct fibers with smaller lattice constant thereby causing reflection of smaller wavelength.

A segment of such fiber was taken and streched to produce all of the visible spectrum. Fig 4.5 shows the tapered fiber. It should be noted that this small section has length of only 1 mm. Therefore, it is not only important for this fibers to have tunable property, but they also exhibit high flexibility at small scales. Measurements were also taken from tapered fiber segment, and normalized spectra are plotted in Fig 4.5 too. Corresponding color at each location gives direct reflection as it is prominent in the plot. Conspicuously, reflection at smaller wavelengths is less evident, this happens because fibers, polymers, just like most materials, start to absorb light in that region.

Figure 4.6: Contact angle setup gives an edge to analyse hydrophobic feature of the samples.

4.1.2 Surface Behaviour Characterization

While producing second step, fibers are inserted into preform in such a way that no additional fiber can fit anymore. By this way, we were aiming to acquire hexagonal distribution and fibers at the edge could arrange in an order leaning to inner surface of the preform. Here, an important aspect of the fabrication method comes into play. Small holes are closed by the surrounding material as they soften and spread around. This feature helped to form complete matrix that holds the rods. However, at the inner edges of the preform, holes were closed not only by embedded matrix (PVDF), but they were also filled with PC, outer material, in particular. In other words, outer layer of the photonic crystal was covered by PC element to some degree. This also helped to protect the rough structure at the edges. After final fiber was drawn, the fibers were etched in DCM chemical to dissolve outer PC layer, leaving those edges cambered, in a way. This was another benefited attribute of the fabrication technique, because with the help of this aspect rough surface was obtained which is expected to promote hydrophobicity of the fibers.

To take contact angle measurements, we utilized an already existing device given in Fig 4.6. This equipment provides a stable ground for samples. A camera

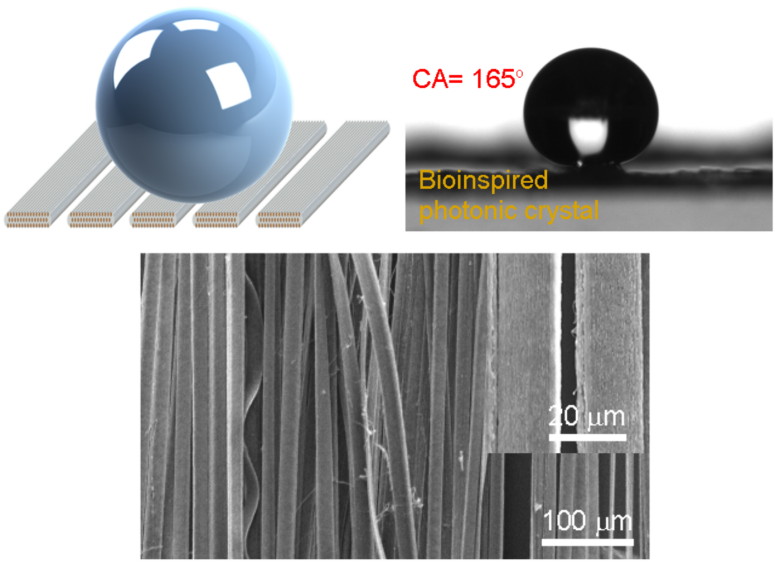

Figure 4.7: Contact angle measurement from assemble of final photonic crystal fibers.

and a light is positioned at opposite sites of this ground. Since light stays behind the sample according to camera, this creates a black portrait of the sample on the screen. This helps for the provided software identify the edges of the sample. When a water droplet is dispensed on the sample, clear and sharp black and white image is taken by the setup, then software finds the contact angle by itself.

Since etched fibers size as small as a few microns, it is impossible for any droplet stand on a single fiber, and also impractical for the software to identify such small scale. To take contact angle measurements we needed to assemble etched fibers in such a way that they form a cluster like in the natural sample, duck feather. For this, we placed multiple fibers side by side, then we etched them together. However, taking this process only one time will give large distances among fibers since fiber sizes get much smaller after etching. To overcome this, we followed this procedure multiple times on the previously etched fibers. Possibility of etching PVDF shell was also taken into account during this action, however PVDF is strong enough to survive multiple DCM exposure.

Contact angle measurements taken from the sample prepared is given in

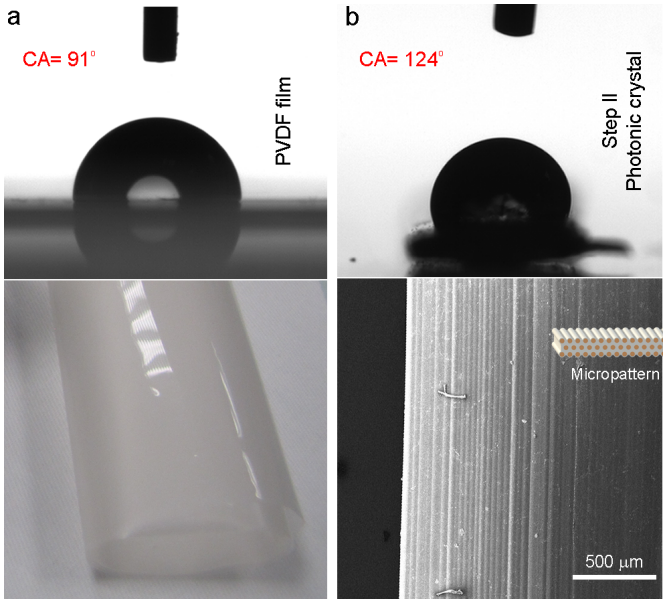

Figure 4.8: Contact angle measurements taken both from film PVDF and second step photonic crystal structure.

Fig 4.7. CA as high as 165° is obtained during this measurements, however multiple measurements suggest CA to be 160±5. To investigate higher hydrophobicity level of produced fibers than naturally existing sample, we take several electron microscopy images from the same specimen used in these measurements. SEM images suggests there to be two orders of roughness on the surface of the fibers. First roughness is the largest one that is the distance between the fibers, the scale of this changes from a few microns to tens of microns. Second order comes from the cambered structure at the edges of the fibers, this was intended during drawing procedure and expected to result in such assistance. In addition, beyond these roughness effects, the main reason to such high hydrophobicity is the PVDF itself. As it was explained in the preceding chapters, fluorinated residues are known to promote hydrophobicity, and here this material also helped to acquire contact angles higher than naturally existing duck feathers.

To further support the idea of roughness effect on PVDF material, we have taken contact angle measurements from second step fibers that has microscale roughness on millimeter scale fiber. Fig 4.8 provides comparison between film and fiber structure of the PVDF. Roughness is known to promote existing feature, in

this case hydrophobicity. CA = 91° of the film is developed to CA = 124° after drawing. 30° increment in one step is repeated in the last step to exceed 150° concluding superhydrophobic fibers.

Chapter 5

Conclusion and Future Work

Fabrication and characterization procedure of bio-inspired two-dimensional photonic crystal fibers, that consist only polymeric materials with compatible glass transition temperature and small refractive index difference, are explained in this thesis. This work concludes the first production of such all-polymer solid-core 2D photonic crystal fibers that possess multi-functional properties; structural coloration and superhydrophobicity.

Investigation of bright and iridescent green-coloration on neck feathers of widely known mallard duck (*Anas Platyrhynchos L.*) revealed that there existed hexagonal distribution of melanin nano-rods along the edges of the keratin barbule elements. Carried out simulations for 2D photonic crystal band-diagram and reflection calculations suggested this distribution as the responsible mechanism for coloration. Such all-polymer solid-core distribution was also discovered in peacock feathers but studies did not go further than analysis due to lack of fabrication approach. Our exploration also implied super-hydrophobicity through surface structure which is considered to help self cleaning of feathers.

After examination, to produce such intricate configuration, we selected iterative size reduction (ISR) due to its applicability to range of polymer materials

and easiness to control nano-scale materials from macro-scale. To imitate multi-functional properties of natural duck feather, polycarbonate (PC) and polyvinyldifluoride (PVDF) materials were selected since they are endowed with close glass transition temperatures and relatively close refractive indices compared to other polymers. In addition, fluoride residues in PVDF are also taken into account as potential for hydrophobicity, and providing nano-scale roughness is considered to promote this feature. However, this work also implies that any thermally compatible polymer pair can be drawn together to form unprecedented fiber structures.

To replicate and see full effect of 2D photonic crystal feature, a unique and novel rectangular hollowed preform was prepared. This helped to increase aspect ratio of the final fibers through which optical and roughness characterization were simplified. This type of production procedure can be established to form differently shaped preforms and fibers to include distinct distributions of nanowires. Green coloration and iridescence properties were satisfactorily mimicked and fibers further characterized to reflect each color in visible spectrum. Through ISR fibers in millimeter to nanometer scales can be produced to operate in a wide range of wavelengths from UV to IR and beyond.

As expected before drawing process, fibers with nanoroughness on PVDF matrix resulted with very high hydrophobicity. It is implied that this production technique also provides control on roughness of overall structures and this could help any type of fiber to have wettability feature. Besides surface structure, being composed of biocompatible polymer materials, this sort of fibers can find its place in textile industry as distinctively colored and wettable featured nonhazardous fibres. In addition, having very thin and iridescent photonic band gap could be used for filtering purposes. Obtaining small spectral linewidths and polarization filtering is possible by careful designs of proposed fibers.

Bibliography

[1] C. F. Bohren, "Understanding colors in nature," *Pigment Cell Research*, vol. 1, pp. 214 – 222, 2006.

[2] S. Kinoshita and S. Yoshioka, "Structural colors in nature: The role of regularity and irregularity in the structure," *Chemphyschem*, vol. 6, pp. 1442 – 1459, 2005.

[3] P. Ball, "Nature's color tricks," *Scientific American*, vol. 306, no. 5, pp. 74 – 79, 2012.

[4] T. W. Goodwin, "Chemistry and biochemistry of plant pigments," *Chemistry and Biochemistry of Plant Pigments*, 1965.

[5] S. Kinoshita, *Structural Colors in the Realm Nature*, vol. 5. 2008.

[6] G. Tayeb, B. Gralak, and S. Enoch, "Structural colors in nature and butterfly-wing modeling," *Optics and Photonics News*, vol. 14, pp. 38 – 43, 2003.

[7] L. Siefferman and G. E. Hill, "UV-blue structural coloration and competition for nestboxes in male eastern bluebirds," *Animal Behaviour*, vol. 69, pp. 67 – 72, 2005.

[8] L. Siefferman and G. E. Hill, "Evidence for sexual selection on structural plumage coloration in female eastern bluebirds (sialia sialis)," *Evolution*, vol. 59, no. 8, pp. 1819–1828, 2005.

[9] L. M. Mäthger, E. J. Denton, N. J. Marshall, and R. T. Hanlon, "Mechanisms and behavioural functions of structural coloration in cephalopods," *Journal of The Royal Society Interface*, vol. 6, pp. 149–163, 2009.

[10] K. Kertész, Z. Bálint, Z. Vértesy, G. Márk, V. Lousse, J.-P. Vigneron, and L. Biró, "Photonic crystal type structures of biological origin: Structural and spectral characterization," *Current Applied Physics*, vol. 6, no. 2, pp. 252 – 258, 2006.

[11] J. W. Galusha, L. R. Richey, J. S. Gardner, J. N. Cha, and M. H. Bartl, "Discovery of a diamond-based photonic crystal structure in beetle scales," *Phys. Rev. E*, vol. 77, p. 050904, 2008.

[12] J. Zi, X. Yu, Y. Li, X. Hu, C. Xu, X. Wang, X. Liu, and R. Fu, "Coloration strategies in peacock feathers," *Proceedings of the National Academy of Sciences*, vol. 100, no. 22, pp. 12576–12578, 2003.

[13] L. P. Biró, Z. Bálint, K. Kertész, Z. Vértesy, G. I. Márk, Z. E. Horváth, J. Balázs, D. Méhn, I. Kiricsi, V. Lousse, and J.-P. Vigneron, "Role of photonic-crystal-type structures in the thermal regulation of a lycaenid butterfly sister species pair," *Phys. Rev. E*, vol. 67, p. 021907, 2003.

[14] L. Rayleigh, "On the maintenance of vibrations by forces of double frequency, and on the propagation of waves through a medium endowed with a periodic structure," *Philosophical Magazine*, vol. 24, pp. 145–159, 1887.

[15] J. P. Vigneron and P. Simonis, "Natural photonic crystals," *Physica B: Condensed Matter*, vol. 407, no. 20, pp. 4032 – 4036, 2012.

[16] P. Vukusic and J. R. Sambles, "Photonic structures in biology," *Nature*, vol. 424, pp. 852 – 855, 2003.

[17] K. Koch, B. Bhushan, and W. Barthlott, "Multifunctional surface structures of plants: An inspiration for biomimetics," *Progress in Materials Science*, vol. 54, no. 2, pp. 137 – 178, 2009.

[18] K. Koch, B. Bhushan, and W. Barthlott, "Diversity of structure, morphology and wetting of plant surfaces," *Soft Matter*, vol. 4, pp. 1943–1963, 2008.

[19] M. Kolle, A. Lethbridge, M. Kreysing, J. J. Baumberg, J. Aizenberg, and P. Vukusic, "Bio-inspired band-gap tunable elastic optical multilayer fibers," *Advanced Materials*, vol. 25, no. 15, pp. 2239–2245, 2013.

[20] Y. Y. Diao and X. Y. Liu, "Controlled colloidal assembly: Experimental modeling of general crystallization and biomimicking of structural color," *Advanced Functional Materials*, vol. 22, no. 7, pp. 1354–1375, 2012.

[21] J. Wang, Y. Zhang, S. Wang, Y. Song, and L. Jiang, "Bioinspired colloidal photonic crystals with controllable wettability," *Accounts of Chemical Research*, vol. 44, no. 6, pp. 405–415, 2011.

[22] K. Liu and L. Jiang, "Bio-inspired design of multiscale structures for function integration," *Nano Today*, vol. 6, no. 2, pp. 155 – 175, 2011.

[23] J. Huang, X. Wang, and Z. L. Wang, "Bio-inspired fabrication of antireflection nanostructures by replicating fly eyes," *Nanotechnology*, vol. 19, no. 2, p. 025602, 2008.

[24] J. J. Walish, Y. Kang, R. A. Mickiewicz, and E. L. Thomas, "Bioinspired electrochemically tunable block copolymer full color pixels," *Advanced Materials*, vol. 21, no. 30, pp. 3078–3081, 2009.

[25] J. D. Joannapoulos, S. G. Johnson, J. N. Winn, and R. D. Meade, *Photonic Crystals: Molding the Flow of Light*. Princeton University Press, second ed., 2008.

[26] H. Kosaka, T. Kawashima, A. Tomita, M. Notomi, T. Tamamura, T. Sato, and S. Kawakami, "Superprism phenomena in photonic crystals," *Phys. Rev. B*, vol. 58, pp. R10096–R10099, 1998.

[27] H. Kubota, S. Kawanishi, S. Koyanagi, M. Tanaka, and S. Yamaguchi, "Absolutely single polarization photonic crystal fiber," *Photonics Technology Letters, IEEE*, vol. 16, no. 1, pp. 182–184, 2004.

[28] S. Noda, M. Yokoyama, M. Imada, A. Chutinan, and M. Mochizuki, "Polarization mode control of two-dimensional photonic crystal laser by unit cell structure design," *Science*, vol. 293, no. 5532, pp. 1123–1125, 2001.

[29] Z.-Y. Li, B.-Y. Gu, and G.-Z. Yang, "Large absolute band gap in 2d anisotropic photonic crystals," *Phys. Rev. Lett.*, vol. 81, pp. 2574–2577, 1998.

[30] P. Yeh, *Optical waves in layered media*. Wiley-Interscience, second ed., 2005.

[31] J. A. Reyes and A. Lakhtakia, "Electrically controlled reflection and transmission of obliquely incident light by structurally chiral materials," *Optics Communications*, vol. 266, no. 2, pp. 565 – 573, 2006.

[32] E. Chow, S. Lin, S. Johnson, P. Villeneuve, J. Joannopoulos, J. Wendt, G. Vawter, W. Zubrzycki, H. Hou, and A. Alleman, "Three-dimensional control of light in a two-dimensional photonic crystal slab," *Nature*, vol. 407, pp. 983 – 986, 2000.

[33] A. Yildirim, M. Vural, M. Yaman, and M. Bayindir, "Bioinspired optoelectronic nose with nanostructured wavelength-scalable hollow-core infrared fibers," *Advanced Materials*, vol. 23, no. 10, pp. 1263–1267, 2011.

[34] Özlem Köylü, "Polymer/glass hollow-core photonic band gap fibers for infrared laser beam delivery," Master's thesis, Bilkent University, 2011.

[35] M. Vural, "Hollow core photonic bandgap fibers for medical applications," Master's thesis, Bilkent University, 2011.

[36] F. Luan, J. Knight, P. Russell, S. Campbell, D. Xiao, D. Reid, B. Mangan, D. Williams, and P. Roberts, "Femtosecond soliton pulse delivery at 800nm wavelength in hollow-core photonic bandgap fibers," *Opt. Express*, vol. 12, no. 5, pp. 835–840, 2004.

[37] R. Bise, R. Windeler, K. S. Kranz, C. Kerbage, B. Eggleton, and D. Trevor, "Tunable photonic band gap fiber," in *Optical Fiber Communication Conference and Exhibit, 2002. OFC 2002*, pp. 466–468, 2002.

[38] F. Luan, A. K. George, T. D. Hedley, G. J. Pearce, D. M. Bird, J. C. Knight, and P. S. J. Russell, "All-solid photonic bandgap fiber," *Opt. Lett.*, vol. 29, no. 20, pp. 2369–2371, 2004.

[39] B. Temelkuran, S. D. Hart, G. Benoit, J. D. Joannopoulos, and Y. Fink, "Wavelength-scalable hollow optical fibres with large photonic bandgaps for co2 laser transmission," *Nature*, vol. 420, pp. 650–653, 2002.

[40] A. B. Seddon, "A prospective for new mid-infrared medical endoscopy using chalcogenide glasses," *International Journal of Applied Glass Science*, vol. 2, no. 3, pp. 177–191, 2011.

[41] O. Majdani, J. Wittkopf, M. S. Dietrich, and R. F. Labadie, "Penetration of co2 laser into the otic capsule using a hand-held, flexible-fiber delivery system," *Lasers in Surgery and Medicine*, vol. 41, no. 7, pp. 509–513, 2009.

[42] S. Wang, "Principles of distributed feedback and distributed bragg-reflector lasers," *Quantum Electronics, IEEE Journal of*, vol. 10, no. 4, pp. 413–427, 1974.

[43] T. F. Krauss, R. M. D. L. Rue, and S. Brand, "Two-dimensional photonic-bandgap structures operating at near-infrared wavelengths," *Nature*, vol. 383, pp. 699–702, 1996.

[44] K. K. Fung, "Photonic iridescence of a blue-banded bee," *Microscopy and Microanalysis*, vol. 11, pp. 1202–1203, 2005.

[45] G. Cook, P. L. Timms, and C. Gltner-Spickermann, "Exact replication of biological structures by chemical vapor deposition of silica," *Angewandte Chemie International Edition*, vol. 42, no. 5, pp. 557–559, 2003.

[46] J. Broeng, S. E. Barkou, A. Bjarklev, J. C. Knight, T. A. Birks, and P. S. Russell, "Highly increased photonic band gaps in silica/air structures," *Optics Communications*, vol. 156, no. 46, pp. 240 – 244, 1998.

[47] P. Russell, "Photonic crystal fibers," *Science*, vol. 299, no. 5605, pp. 358–362, 2003.

[48] E. Yablonovitch, "Inhibited spontaneous emission in solid-state physics and electronics," *Phys. Rev. Lett.*, vol. 58, pp. 2059–2062, 1987.

[49] E. Yablonovitch, T. J. Gmitter, and K. M. Leung, "Photonic band structure: The face-centered-cubic case employing nonspherical atoms," *Phys. Rev. Lett.*, vol. 67, pp. 2295–2298, 1991.

[50] K. M. Ho, C. T. Chan, and C. M. Soukoulis, "Existence of a photonic gap in periodic dielectric structures," *Phys. Rev. Lett.*, vol. 65, pp. 3152–3155, 1990.

[51] A. Argyros, S. Manos, M. Large, D. McKenzie, G. Cox, and D. Dwarte, "Electron tomography and computer visualisation of a three-dimensional photonic crystal in a butterfly wing-scale," *Micron*, vol. 33, no. 5, pp. 483 – 487, 2002.

[52] K. Michielsen and D. Stavenga, "Gyroid cuticular structures in butterfly wing scales: biological photonic crystals," *Journal of The Royal Society Interface*, vol. 5, no. 18, pp. 85–94, 2008.

[53] P. Vukusic, J. R. Sambles, C. R. Lawrence, and R. J. Wootton, "Quantified interference and diffraction in single morpho butterfly scales," *Proceedings of the Royal Society of London. Series B: Biological Sciences*, vol. 266, no. 1427, pp. 1403–1411, 1999.

[54] T. Khudiyev, T. Dogan, and M. Bayindir, "Biomimicry of multifunctional nanostructures in the neck feathers of mallard (anas platyrhynchos l.) drakes," *Sci. Rep.*, vol. 4, 2014.

[55] J. W. Galusha, L. R. Richey, M. R. Jorgensen, J. S. Gardner, and M. H. Bartl, "Study of natural photonic crystals in beetle scales and their conversion into inorganic structures via a sol-gel bio-templating route," *J. Mater. Chem.*, vol. 20, pp. 1277–1284, 2010.

[56] A. Malshe, K. Rajurkar, A. Samant, H. N. Hansen, S. Bapat, and W. Jiang, "Bio-inspired functional surfaces for advanced applications," {*CIRP*} *Annals - Manufacturing Technology*, vol. 62, no. 2, pp. 607 – 628, 2013.

[57] S. Nishimoto and B. Bhushan, "Bioinspired self-cleaning surfaces with superhydrophobicity, superoleophobicity, and superhydrophilicity," *RSC Adv.*, vol. 3, pp. 671–690, 2013.

[58] M. J. Hancock, K. Sekeroglu, and M. C. Demirel, "Bioinspired directional surfaces for adhesion, wetting, and transport," *Advanced Functional Materials*, vol. 22, no. 11, pp. 2223–2234, 2012.

[59] M. Liu, S. Wang, Z. Wei, Y. Song, and L. Jiang, "Bioinspired design of a superoleophobic and low adhesive water/solid interface," *Advanced Materials*, vol. 21, no. 6, pp. 665–669, 2009.

[60] R. N. Wenzel, "Surface roughness and contact angle.," *The Journal of Physical and Colloid Chemistry*, vol. 53, no. 9, pp. 1466–1467, 1949.

[61] T. Sun, L. Feng, X. Gao, and L. Jiang, "Bioinspired surfaces with special wettability," *Accounts of Chemical Research*, vol. 38, no. 8, pp. 644–652, 2005.

[62] D. ner and T. J. McCarthy, "Ultrahydrophobic surfaces. effects of topography length scales on wettability," *Langmuir*, vol. 16, no. 20, pp. 7777–7782, 2000.

[63] E. Pierce, F. Carmona, and A. Amirfazli, "Understanding of sliding and contact angle results in tilted plate experiments," *Colloids and Surfaces A: Physicochemical and Engineering Aspects*, vol. 323, no. 13, pp. 73 – 82, 2008.

[64] Z. Yoshimitsu, A. Nakajima, T. Watanabe, and K. Hashimoto, "Effects of surface structure on the hydrophobicity and sliding behavior of water droplets," *Langmuir*, vol. 18, no. 15, pp. 5818–5822, 2002.

[65] M. Callies and D. Quere, "On water repellency," *Soft Matter*, vol. 1, pp. 55–61, 2005.

[66] H. Budunoglu, A. Yildirim, M. O. Guler, and M. Bayindir, "Highly transparent, flexible, and thermally stable superhydrophobic ormosil aerogel thin films," *ACS Applied Materials and Interfaces*, vol. 3, no. 2, pp. 539–545, 2011.

[67] P. J. van Zwol, G. Palasantzas, and J. T. M. De Hosson, "Influence of roughness on capillary forces between hydrophilic surfaces," *Phys. Rev. E*, vol. 78, p. 031606, 2008.

[68] J. Lai, B. Sunderland, J. Xue, S. Yan, W. Zhao, M. Folkard, B. D. Michael, and Y. Wang, "Study on hydrophilicity of polymer surfaces improved by plasma treatment," *Applied Surface Science*, vol. 252, no. 10, pp. 3375 – 3379, 2006.

[69] L. Ponsonnet, K. Reybier, N. Jaffrezic, V. Comte, C. Lagneau, M. Lissac, and C. Martelet, "Relationship between surface properties (roughness, wettability) of titanium and titanium alloys and cell behaviour," *Materials Science and Engineering: C*, vol. 23, no. 4, pp. 551 – 560, 2003.

[70] W. Choi, A. Tuteja, S. Chhatre, J. M. Mabry, R. E. Cohen, and G. H. McKinley, "Fabrics with tunable oleophobicity," *Advanced Materials*, vol. 21, no. 21, pp. 2190–2195, 2009.

[71] C. Aulin, J. Netrval, L. Wagberg, and T. Lindstrom, "Aerogels from nanofibrillated cellulose with tunable oleophobicity," *Soft Matter*, vol. 6, pp. 3298–3305, 2010.

[72] W. Barthlott and C. Neinhuis, "Purity of the sacred lotus, or escape from contamination in biological surfaces," *Planta*, vol. 202, no. 1, pp. 1–8, 1997.

[73] X. Zhang, F. Shi, J. Niu, Y. Jiang, and Z. Wang, "Superhydrophobic surfaces: from structural control to functional application," *J. Mater. Chem.*, vol. 18, pp. 621–633, 2008.

[74] H. F. Bohn and W. Federle, "Insect aquaplaning: Nepenthes pitcher plants capture prey with the peristome, a fully wettable water-lubricated anisotropic surface," *Proceedings of the National Academy of Sciences of the United States of America*, vol. 101, no. 39, pp. 14138–14143, 2004.

[75] Y. Wu, H. Yan, M. Huang, B. Messer, J. H. Song, and P. Yang, "Inorganic semiconductor nanowires: Rational growth, assembly, and novel properties," *Chemistry A European Journal*, vol. 8, no. 6, pp. 1260–1268, 2002.

[76] E. Latu-Romain, P. Gilet, P. Noel, J. Garcia, P. Ferret, M. Rosina, G. Feuillet, F. Lvy, and A. Chelnokov, "A generic approach for vertical integration of nanowires," *Nanotechnology*, vol. 19, no. 34, p. 345304, 2008.

[77] A. I. Hochbaum, R. Fan, R. He, and P. Yang, "Controlled growth of si nanowire arrays for device integration," *Nano Letters*, vol. 5, no. 3, pp. 457–460, 2005.

[78] L. Vayssieres, "Growth of arrayed nanorods and nanowires of zno from aqueous solutions," *Advanced Materials*, vol. 15, no. 5, pp. 464–466, 2003.

[79] Y. Wu, R. Fan, and P. Yang, "Block-by-block growth of single-crystalline si/sige superlattice nanowires," *Nano Letters*, vol. 2, no. 2, pp. 83–86, 2002.

[80] J. Hu, T. W. Odom, and C. M. Lieber, "Chemistry and physics in one dimension: Synthesis and properties of nanowires and nanotubes," *Accounts of Chemical Research*, vol. 32, no. 5, pp. 435–445, 1999.

[81] K. M. Ryan, D. Erts, H. Olin, M. A. Morris, and J. D. Holmes, "Three dimensional architectures of ultra-high density semiconducting nanowires deposited on chip," *Journal of the American Chemical Society*, vol. 125, no. 20, pp. 6284–6288, 2003.

[82] D. V. Talapin, C. T. Black, C. R. Kagan, E. V. Shevchenko, A. Afzali, and C. B. Murray, "Alignment, electronic properties, doping, and on-chip growth of colloidal pbse nanowires," *The Journal of Physical Chemistry C*, vol. 111, no. 35, pp. 13244–13249, 2007.

[83] J. Shui and J. C. M. Li, "Platinum nanowires produced by electrospinning," *Nano Letters*, vol. 9, no. 4, pp. 1307–1314, 2009.

[84] C. Zhu, Y. Yu, L. Gu, K. Weichert, and J. Maier, "Electrospinning of highly electroactive carbon-coated single-crystalline lifepo4 nanowires," *Angewandte Chemie International Edition*, vol. 50, no. 28, pp. 6278–6282, 2011.

[85] M. Yaman, T. Khudiyev, E. Ozgur, M. Kanik, O. Aktas, E. O. Ozgur, H. Deniz, E. Korkut, and M. Bayindir, "Arrays of indefinitely long uniform nanowires and nanotubes," *Nat. Materials*, vol. 10, no. 7, pp. 494–501, 2011.

[86] T. Khudiyev, E. Ozgur, M. Yaman, and M. Bayindir, "Structural coloring in large scale coreshell nanowires," *Nano Letters*, vol. 11, no. 11, pp. 4661–4665, 2011.

[87] E. Ozgur, O. Aktas, M. Kanik, M. Yaman, and M. Bayindir, "Macroscopic assembly of indefinitely long and parallel nanowires into large area photodetection circuitry," *Nano Letters*, vol. 12, no. 5, pp. 2483–2487, 2012.